Meteoritics & Planetary Science 39, Nr 9, 1555–1575 (2004)
Abstract available online at http://meteoritics.org

New findings for the equilibrated enstatite chondrite Grein 002

Andrea PATZER,[1*] Jochen SCHLÜTER,[2] Ludolf SCHULTZ,[3] Mahmud TARKIAN,[2]
Dolores H. HILL,[1] and William V. BOYNTON[1]

[1]Lunar and Planetary Laboratory, University of Arizona, Tucson, Arizona 85721, USA
[2]Mineralogisches Museum und Mineralogisch-Petrographisches Institut der Universität Hamburg, D-20146 Hamburg, Germany
[3]Max-Planck-Institut für Chemie, D-55020 Mainz, Germany
[*]Corresponding author. E-mail: apatzer@lpl.arizona.edu

(Received 20 June 2003; revision accepted 10 July 2004)

Abstract–We report new petrographic and chemical data for the equilibrated EL chondrite Grein 002, including the occurrence of osbornite, metallic copper, abundant taenite, and abundant diopside. As inferred from low Si concentrations in kamacite, the presence of ferroan alabandite, textural deformation, chemical equilibration of mafic silicates, and a subsolar noble gas component, we concur with Grein 002's previous classification as an EL4–5 chondrite. Furthermore, the existence of pockets consisting of relatively coarse, euhedral enstatite crystals protruding large patches of Fe-Ni alloys suggests to us that this EL4–5 chondrite has been locally melted. We suspect impact induced shock to have triggered the formation of the melt pockets.

Mineralogical evidence indicates that the localized melting of metal and adjacent enstatite must have happened relatively late in the meteorite's history. The deformation of chondrules, equilibration of mafic silicates, and generation of normal zoning in Fe, Zn-sulfides took place during thermal alteration before the melting event. Following parent body metamorphism, daubreelite was exsolved from troilite in response to a period of slow cooling at subsolidus temperatures. Exsolution of schreibersite from the coarse metal patches probably occurred during a similar period of slow cooling subsequent to the event that induced the formation of the melt pockets. Overall shock features other than localized melting correspond to stage S2 and were likely established by the final impact that excavated the Grein 002 meteoroid.

INTRODUCTION

Enstatite chondrites (ECs) are highly reduced meteorites that mainly consist of Mg-pyroxene (enstatite), metal (kamacite), and Fe-sulfide (troilite) (Keil 1968). The enstatite contains only very low concentrations of FeO, and the metal phase exhibits relatively high Si abundances. Both characteristics are a consequence of very low O_2 fugacities during condensation and accretion of the enstatite chondrite parent body (e.g., Larimer and Bartholomay 1979; Brearley and Jones 1998). Due to the reducing conditions, special forms of sulfides and several unusual types of minerals like phosphides and nitrides occur in minor or accessory amounts (e.g., Keil 1989, and references therein).

With respect to the iron content, two subgroups can be distinguished: EH chondrites (with H for high iron) and EL chondrites (with L for low iron) (e.g., Sears 1980; Sears et al. 1982; Hertogen et al. 1983; Weeks and Sears 1985; Kallemeyn and Wasson 1986). According to the classification scheme of Van Schmus and Wood (1967), ECs include all petrologic types from 3 to 7. The exact genetic links between EL and EH chondrites and among the petrologic types, however, remain enigmatic. Due to relatively large variations in chemical composition and textural features, the classification of E chondritic samples often proves to be more difficult than that of ordinary chondrites, and reclassifications are not unusual (e.g., Kallemeyn and Wasson 1986; Zhang et al. 1995; Lin and Kimura 1997; Rubin and Scott 1997; Rubin et al. 1997).

We present comprehensive petrologic and noble gas data on an equilibrated EL chondrite, Grein 002. This meteorite, a single stone of 609 g, was recovered during an expedition of the German magazine *GEO* in cooperation with the Mineralogical Museum Hamburg (Germany) and the Max-Planck-Institut für Chemie in Mainz (Germany) in the Ténéré du Tafassâsset, a part of the central Sahara located in the northeast of the Republic of Niger, at 20º42′52″N/11º06′57″E. The date of the find was March 3, 1997. In the following year,

Grein 002 was listed as an EL4–5 chondrite in *The Meteoritical Bulletin* (Grossman 1998). An investigation of its cosmogenic radionuclides revealed that Grein 002 must have been a recent fall (Schultz et al. 1998). We revisit the question of its taxonomical position and, based on our findings, give a detailed petrographic description of the meteorite. In addition, we address its noble gas record and interpret its mineralogical and chemical inventory in terms of pre- and post-accretionary events. The evolution of Grein 002 was more complex than the simple assignment EL4–5 suggests.

We also present new reflectance and micro hardness data of opaque mineral phases. In this context, we note that Grein 002 contains a cubic Fe, Zn-sulfide instead of sphalerite (Zn, Fe-sulfide). In the literature (e.g., Lin and Goresy 2002), both Fe, Zn- and Zn, Fe-sulfides in ECs have been collectively called sphalerite. According to the definitions of the International Mineralogical Association (Nickel 1992), however, a distinction should be made. We were not able to obtain complete structural data on this so far unrecognized Fe, Zn-sulfide due to its small grain size. Consequently, the requirements for approval as a new mineral by the Commission on New Minerals and Mineral Names are not met at this point. Therefore, we simply refer to it as the Fe-rich equivalent of sphalerite.

ANALYTICAL TECHNIQUES

Petrography and Bulk and Mineral Analyses

Two thin sections of Grein 002 were prepared for the microscopic study and the electron microprobe measurements of the rock. In addition, four individual chips were broken off of a subsample for INAA. Two of these samples (0.1979 and 1.1231 g, respectively) were irradiated and counted at the neutron activation facility of the Max-Planck-Institut für Chemie in Mainz, Germany, in 1997. At that time, the bulk chemical analysis was carried out in connection with the original classification of Grein 002 (Grossman 1998). The procedure applied for this first INAA investigation of Grein 002 has been reported by Zipfel et al. (2000). Peak deconvolution of the spectra recorded in Mainz was carried out according to Kruse (1979). The other two specimen (0.1771 and 0.1344 g) were investigated using the neutron activation facilities at the University of Arizona in Tucson in 2003. Details on the parameters and techniques involved in the INAA procedure applied in Tucson have been given by Patzer et al. (2004). Table 1 shows the elemental concentrations obtained by INAA.

The two thin sections were examined by optical microscope and electron microprobe. The microscopic investigation was conducted to determine the weathering grade and shock stage of Grein 002 and to distinguish opaque minerals and learn about the optical properties of the existing mineral phases. Subsequently, the thin sections were, in part, analyzed by means of a Cameca Camebax Microbeam wavelength-dispersive electron microprobe at the Department for Mineralogy and Petrology of the Universtität Hamburg. Operation conditions were set to 20 kV and 25 nA. The kα X-ray lines were used for all elements. Pure elements (Ni and Co), andradite (for Ca and Si), apatite (for P), vanadinite (for V), as well as synthetic MgO (for Mg), Al_2O_3 (for Al), ZnS (for Zn and S), $MnTiO_3$ (for Ti and Mn), Cr_2O_3 (for Cr), and FeS_2 (for Fe) were selected as standards. For data corrections, we used the PAP online programs (Pouchon and Pichoir 1991). A point count evaluation of a 13 × 10 mm polished section area provided the data for the modal mineral content of Grein 002. Further microprobe analyses were performed at the Lunar and Planetary Laboratory with a Cameca SX-50 electron microprobe according to the procedures described in Patzer et al. (2004; see also Kring et al. 1996). N concentrations were obtained by applying a boron nitride standard and by setting the SX-50 at 15 kV, 40 nA, and 60 sec using the PC1 crystal with a reflection angle of ±7500 sinθ for the background. All microprobe data are compiled in Tables 2, 3a, and 3b. The analyses results produced in Tucson and Hamburg are identical within uncertainties for all mineral phases except P in schreibersite. Here, somewhat higher values were determined in Tucson (15.9 ± 0.2 wt% versus 13.2 ± 0.4 wt%).

Vickers Micro Hardness and Reflectance Data

To determine reflectance properties of the opaque minerals and oldhamite in Grein 002, we used a computerized ZEISS MPM micro photometer with WTiC standard (R_{589} in air = 49.5%, R_{589} in oil = 35.5%) and SiC standard (R_{589} in air = 20.3%, R_{589} in oil = 7.3%). Details of this technique have been elucidated by Tarkian and Bernhardt (1984). The Vickers hardness (VHN) was determined with a Leitz Durimet. Both VHN and reflectance data are listed in Tables 4a and 4b. All values represent the average result of several measurements of central grain areas.

Noble Gases

The concentrations and isotopic compositions of the noble gases were determined by means of an all-metal mass spectrometer and one-step pyrolysis at ~1700 °C. Before the extraction of the rare gases, the bulk material was pre-heated in vacuo to a maximum of 120 °C for at least 24 hr to reduce adsorbed atmospheric noble gases. For the analysis, a single chip free of fusion crust and weighing 80.65 mg was broken off of a subsample. In addition, two aliquants (62.03 and 63.68 mg) were prepared that mainly consisted of melt. All specimens were then wrapped into Ni foil. For details on the instrumentation and procedure see Scherer at al. (1998) and Loeken et al. (1992). The uncertainties of gas concentrations vary from 5 to 10% for He, Ne, and Ar and from 10 to 15% for Kr and Xe. The measured concentrations of ^{84}Kr, ^{129}Xe, and

Table 1. Elemental concentrations of Grein 002.[a]

	0.6605 g (Mainz)	Uncertainty	0.1557 g (Tucson)	Uncertainty	Mean EH[b]	Mean EL[b]
Na	6880	3	6265	1	6800	5800
Mg	–	–	15.2	3	10.6	14.1
Al	–	–	1.29	2	0.81	1.05
Si	–	–	20.0[c]	10	16.7	18.6
K	758	5	720	3	800	735
Ca	0.80	20	1.08	9	0.85	1.01
Sc	7.37	3	7.57	2	5.7	7.4
Ti	<2000	–	<1650	–	450	580
V	–	–	49.9	4	54	60
Cr	2770	3	2544	1	3150	3050
Mn	1760	3	1735	8	2200	1630
Fe	23.51	3	25.14	1	29	22
Co	689	3	747	1	840	670
Ni	17200	4	17260	1	17500	13000
Zn	200	7	190	3	250	17
Ga	11.4	7	11.8	5	16	11
As	2.4	5	2.40	6	3.45	2.20
Se	18.2	5	17.5	3	25.5	13.5
Br	–	–	1.50	6	2.4	0.8
Rb	–	–	5.5	20	2.6	2.5
Ru	–	–	0.93	23	0.915	0.831
Sb	0.127	20	0.115	6	0.196	0.090
La	0.21	12	0.368	8	0.235	0.190
Sm	0.133	5	0.198	2	0.140	0.135
Eu	0.063	25	0.070	21	0.054	0.054
Yb	0.160	12	0.320	30	0.160	0.165
Lu	0.026	20	0.029	25	0.024	0.024
W	–	–	0.21	20	–	–
Re	0.074	15	0.054	12	0.052	0.047
Os	0.658	7	0.755	12	0.654	0.589
Ir	0.596	3	0.618	1	0.565	0.525
Au	0.23	3	0.241	1	0.330	0.225
C[d]	0.5296	–	0.5605	–	0.4	0.36
N[d]	0.0530	–	0.0516	–	–	–

[a]Concentrations are in µg/g except for Mg, Al, Fe, Ca (%).
[b]Data taken from Wasson and Kallemeyn (1988).
[c]Value has been derived from microprobe analyses.
[d]Carbon and nitrogen data (in %) were determined from two different aliquants of Grein 002 by R. Seifert (Hamburg) using Element Analyser Carlo Erba NA 1500; the detection limits for C and N were 0.05% and 0.01%, respectively.

^{132}Xe are assumed to be entirely trapped. Trapped ^{36}Ar abundances, on the other hand, were calculated by subtracting a cosmogenic contribution from the measured amount of ^{36}Ar ($^{36}Ar_c = 0.65 \times {}^{38}Ar_c$; Wieler 2002). The trapped ratios ^{36}Ar/^{132}Xe and ^{84}Kr/^{132}Xe are believed to be known to better than 20%.

Production rates and cosmic ray exposure ages (CREA) were calculated according to Eugster (1988; see also Scherer at al. 1998). Individual elemental abundances as obtained from the INAA analyses were applied to account for chemical differences from L chondrites and to adopt the production rates to the meteorite's composition. The calculated correction factors are 0.993 for cosmogenic ^{3}He, 0.831 for cosmogenic ^{21}Ne, and 0.836 for cosmogenic ^{38}Ar.

For the evaluation of gas retention ages, we used average U and Th concentrations (Mason 1979) and K concentrations gained from the INAA analyses. Furthermore, we applied a correction for cosmogenic ^{4}He with $^{4}He_c = 5 \times {}^{3}He_c$ (Heymann 1967). Relevant noble gas concentrations and ratios as well as exposure and gas retention ages are compiled in Table 5.

RESULTS AND DISCUSSION

Petrographic Description Including Weathering Degree and Shock Stage

Grein 002 was completely covered with fusion crust and macroscopically exhibited a fresh appearance (Fig. 1). The

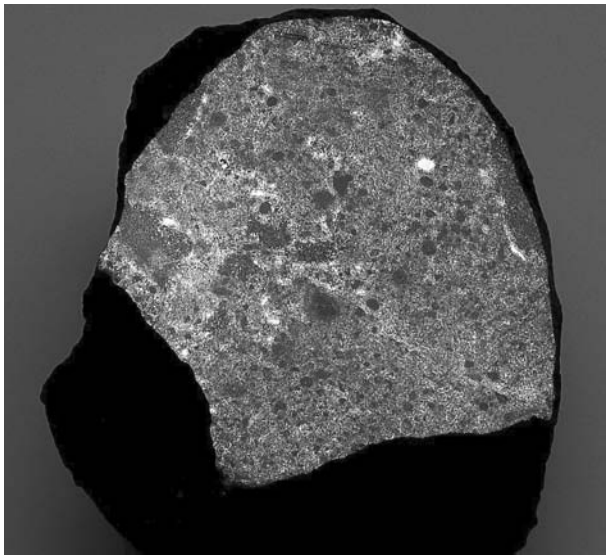

Fig. 1. Photograph of the Grein 002 meteorite (cut surface is about 4.5 × 5.0 cm). A few intact chondrules are readily recognizable. The darker colored, clast-like areas (e.g., on the right and left edge, respectively) are melt pockets consisting of relatively coarse-grained, euhedral enstatite and large patches of Fe, Ni-metal (see Figs. 3 and 4). We believe that these pockets were produced by shock-induced localized melting of the rock. Additional shock features identified in Grein 002 include silicate darkening, weak undulose extinction, fracturing, and one diffuse opaque vein (Photo: K. C. Lyncker, Hamburg).

microscopic investigation confirms this assessment and reveals a low weathering grade of W1. The mineral phase most susceptible to terrestrial alteration in enstatite chondrites is oldhamite (Ramdohr 1973). Oldhamite in Grein 002 has grain sizes of up to 70 μm and occurs either as individual, often rounded crystals, loose clusters, or in close association with opaque phases. The bigger grains show good cleavage and bright (yellowish) internal reflections. Only the smaller grains tend to exhibit signs of incipient or even advanced corrosion. The metal phase, which is more resistant to weathering in enstatite chondrites than in ordinary chondrites due to its relatively high Si content, displays only minor rims of oxidation, if any, and only a few small limonitic veins are present.

With respect to shock features, we observed weak undulose extinction (with an angle discrepancy of only a few degrees) and sets of planar fractures in some enstatite grains. We also noticed finely dispersed opaque inclusions within many silicate crystals as well as a single diffuse opaque vein at the edge of one of the thin sections. The dispersion of sub-μm-sized sulfide and/or metal inclusions causes the phenomenon of silicate darkening but is not indicative of a particular shock stage. All other observed shock attributes correspond to weak shock at stage S2 (Rubin et al. 1997).

In addition to shock alteration, the meteorite apparently underwent considerable thermal metamorphism leading to the deformation of chondrules. Most chondrules are turned into poorly delineated "ghosts" (Fig. 2). In some instances, they also display deformed, elongated shapes. Others occur only as fragments. Two different chondrule types can be distinguished, exhibiting either radial pyroxene or rare porphyritic textures. Silicate phases identified in chondrules of Grein 002 are orthopyroxene (enstatite), clinopyroxene (diopside), feldspar (plagioclase), and minor olivine (forsterite). They show subhedral or anhedral crystal shapes and small grain sizes (<100 μm). In some cases, kamacite and troilite form ubiquitous tiny opaque inclusions throughout the chondrule body. While chondrule and chondrule fragment sizes vary, the biggest intact chondrule measured 2 mm across.

In reflected light, we can distinguish 9 opaque phases including kamacite, taenite, troilite, schreibersite, daubreelite, alabandite, a sphalerite-like sulfide, osbornite, and at least two small grains of native copper. Despite its scarcity and very small size (1–10 μm), osbornite turns out to be readily detectable, exhibiting a bright yellow color and distinct shape (see also Ramdohr 1973). It is always associated with troilite, kamacite, or taenite. Its polishing hardness is similar to that of kamacite, while its Vickers micro hardness (VHN) has been determined to be only 150. Kamacite grains yield a VHN of 214–251 (VHN values of present opaque phases and oldhamite are given in Table 4a). Aside from the few tiny crystals of Fe-bearing osbornite (TiN; Tables 3a and 3b), we also observed the (transparent) silicon oxynitride sinoite (Si_2N_2O).

The metal phase of Grein 002 is heterogeneously distributed. Some areas including the chondrules are remarkably opaque-poor. Other areas appear metal-poor but are rich in troilite. Kamacite, taenite, and troilite can often be found as individual crystals (~10–100 μm). All other sulfides always coexist with either troilite or Fe-Ni grains or both to form complex interstitial assemblages. One of those sulfides, daubreelite, commonly emerges as exsolution lamellae in troilite. We detected only one euhedral daubreelite crystal surrounded by troilite. In addition, rare, very fine, second-generation exsolution lamellae of troilite in daubreelite have been identified (see also Ramdohr 1973). All sulfide phases are fine-grained and span a size range of only 10 to 50 μm (max. 70 μm for alabandite). The size of troilite crystals varies from a few to ~100 μm.

One of the distinctive attributes of Grein 002 is related to the occurrence of melt pockets. Aside from metamorphism, this enstatite chondrite appears to have experienced localized melting. The melt pockets are sub-mm to cm-sized and ubiquitous. They consist of euhedral enstatite that protrudes or is enclosed by up to 2 mm-large patches of metal (Fig. 3). This particular type of texture suggests crystallization from a melt. The relatively coarse crystalline appearance of the melt pockets stands in contrast to the dominating anhedral, fine-grained, and chondritic nature of Grein 002. Similar coarse-crystalline intergrowths of euhedral enstatite and kamacite have been reported for the enstatite chondrite melt rocks

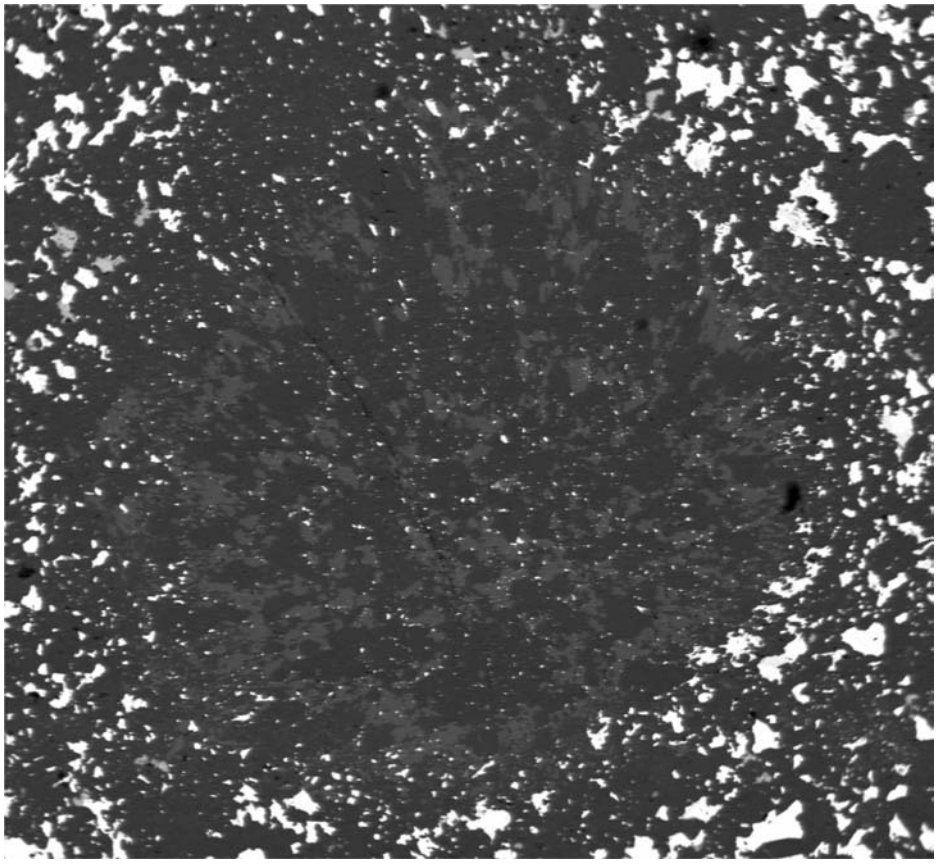

Fig. 2. Photomicrograph of a partially resorbed chondrule in Grein 002 (chondrule diameter is ~600 μm). The phases present in the chondrule are enstatite (dark grey) and diopside (medium grey) as well as minor plagioclase, sulfides, and metal. The deformation of the chondrule indicates thermal overprinting of the rock. The overall appearance of chondrules in Grein 002 supports the meteorite's classification as an E4–5 chondrite (see Grossman 1998).

Ilafegh 009 (McCoy et al. 1995) and Y-86004 (Lin and Kimura 1998) and for the impact melt breccia Abee (Rubin and Scott 1997). In all three cases, the pyroxene-metal assemblages crystallized relatively rapidly from a melt that was most likely formed by impact.

The coarse kamacite patches of the melt areas in Grein 002 occasionally contain schreibersite crystals that reach up to 50 μm in size. In addition to schreibersite, we identified tiny inclusions and minor occurrences of troilite, an Fe phase with variable Si concentrations (up to 35 wt% Si), and graphite. Graphite, in fact, is present not only as inclusions in the coarse kamacite patches but primarily as either sub-mm sized lathy aggregates or as a small, μm-sized interstitial phase closely associated with the metal phase (Fig. 4).

Grein 002 displays at least two occurrences of native copper. This may be the first report of metallic Cu in an enstatite chondrite. Ramdohr (1963) performed a detailed survey of opaque minerals in 135 stony meteorites, with six enstatite chondrites among them. He identified native Cu in "at least 50%" of his sample suite, however, without specifying the respective meteorites. Rubin (1994) noted that metallic Cu occurs in "at least 66%" of ordinary chondrites. In Grein 002, we found one irregular Cu grain of 7 μm that is attached to a metal-sulfide assemblage containing alabandite, troilite, daubreelite, kamacite, and taenite (Fig. 5). The second grain (~6 μm) is situated adjacent to kamacite and troilite. Rubin (1994) has discussed the hypothesis of an impact origin of metallic Cu in ordinary chondrites. We also suspect Grein 002 to be altered by shock. The two occurrences of metallic Cu, however, are linked to unaffected, primary mineral assemblages and are likely of primary origin as well.

In modal terms, Grein 002 consists of 71.9 vol% transparent mineral phases and 27.5 vol% opaque minerals. The former include 44.5 vol% enstatite, 11.5 vol% diopside, 10.5 vol% plagioclase, 3.4 vol% oldhamite, ~1 vol% sinoite, and <1 vol% forsterite. The opaques are 13.8 vol% metal, 10.0 vol% troilite, 2.2 vol% other sulfides, and 1.5 vol% graphite. Limonitic veins account for <1 vol% of the specimen.

Mineral Chemistry and Petrologic Evidence

Major Silicates

As in other enstatite chondrites, the predominant mineral component of Grein 002, enstatite, is very low in FeO

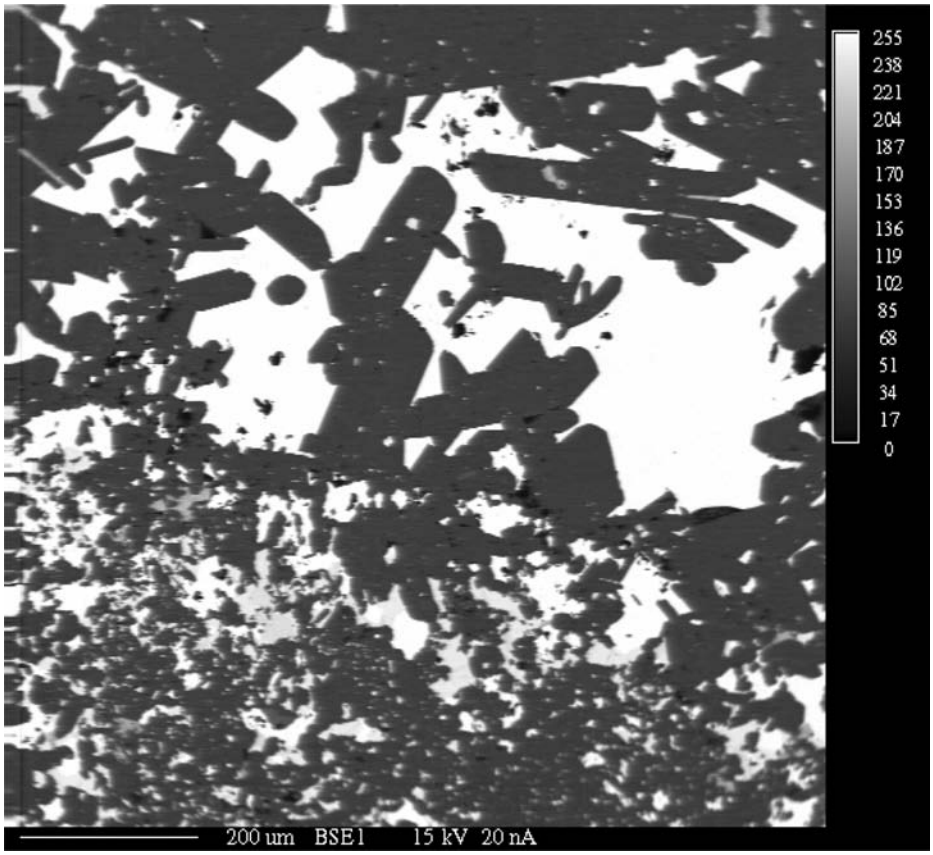

Fig. 3. Photomicrograph depicting the two contrasting lithologies present in Grein 002: coarse-grained enstatite-metal assemblages that we interpret as impact shock-produced melt pockets and fine-grained subhedral to anhedral chondritic material (field of view is ~800 × 1000 μm). The euhedral enstatite crystals (dark grey) protruding large patches of Fe, Ni-metal (bright areas) are up to 200 μm long and exhibit normal igneous Fe zoning. Experimentally constrained crystal growth rates (e.g., Spry 1969; Dowty 1980) suggest that enstatite grains of that size can precipitate from a melt within 10s of seconds. The black phase visible in the image is graphite (see also Fig. 4).

(usually well below 1 oxide%). The average modal composition of the pyroxene is $En_{98.0 \pm 0.4}Wo_{1.3 \pm 0.2}Fs_{0.64 \pm 0.41}$ and shows only small standard deviations (except for ferrosilite, see below). Other major silicate phases are albitic plagioclase and unusually abundant diopside. Diopside is commonly rare in enstatite chondrites and has been reported in minor quantities only for some unquilibrated E3 chondrites and one EL6 specimen (Fogel 1995; Floss et al. 2003). Its formation in the EL6 chondrite EET 90102 has been linked to the metamorphic reaction (Fogel 1997):

$$CaS_{\text{(oldhamite)}} + Mg_2Si_2O_{6\text{ (enstatite)}} = CaMgSi_2O_{6\text{ (diopside)}} + MgS_{\text{(in alabandite)}}$$

Recent REE analyses performed by Floss et al. (2003) are consistent with this hypothesis. The comparatively high content of diopside in Grein 002 (as an equilibrated enstatite chondrite) also may be explained by the above metamorphic reaction. In addition, it supports the idea of aubrite petrogenesis through the melting of diopside-bearing enstatite chondrite material (Fogel 1997; Floss et al. 2003).

Like the chemical composition of enstatite, that of diopside in Grein 002 turns out to be relatively homogeneous except for Fe ($En_{53.6 \pm 0.7}Wo_{46.0 \pm 0.8}Fs_{0.39 \pm 0.21}$; Table 2). As opposed to the mafic silicates, the analyzed feldspars exhibit a significant variability in their major elemental concentrations ($Ab_{82.2 \pm 3.3}An_{13.5 \pm 4.2}Or_{4.37 \pm 1.10}$; Table 2). The chemical heterogeneity probably can be attributed to abundant sub-μm-sized inclusions.

We observed a slight compositional difference between the fine-grained enstatite of chondrules and matrix and the coarse-grained, euhedral enstatite crystals. The latter pyroxenes show a somewhat higher FeO content ($Fs_{>0.5}$ as opposed to $Fs_{<0.5}$ in the former cases). In addition, the euhedral enstatite associated with the large kamacite patches often exhibits zoning, with Fe concentrations increasing from the center toward the rim (Fig. 6). Distinct from Fe, Mg abundances remain constant throughout the grains.

The trend in Fe concentrations in euhedral enstatite of Grein 002 resembles normal igneous zoning and was most likely established when the melt pockets formed, thus strengthening the case of melting as opposed to solid state recrystallization. However, unlike other enstatite melt rocks and breccias (e.g., Ilafegh 009, Y-86004, and Abee; see McCoy et al. 1995; Lin and Kimura 1998; Rubin and

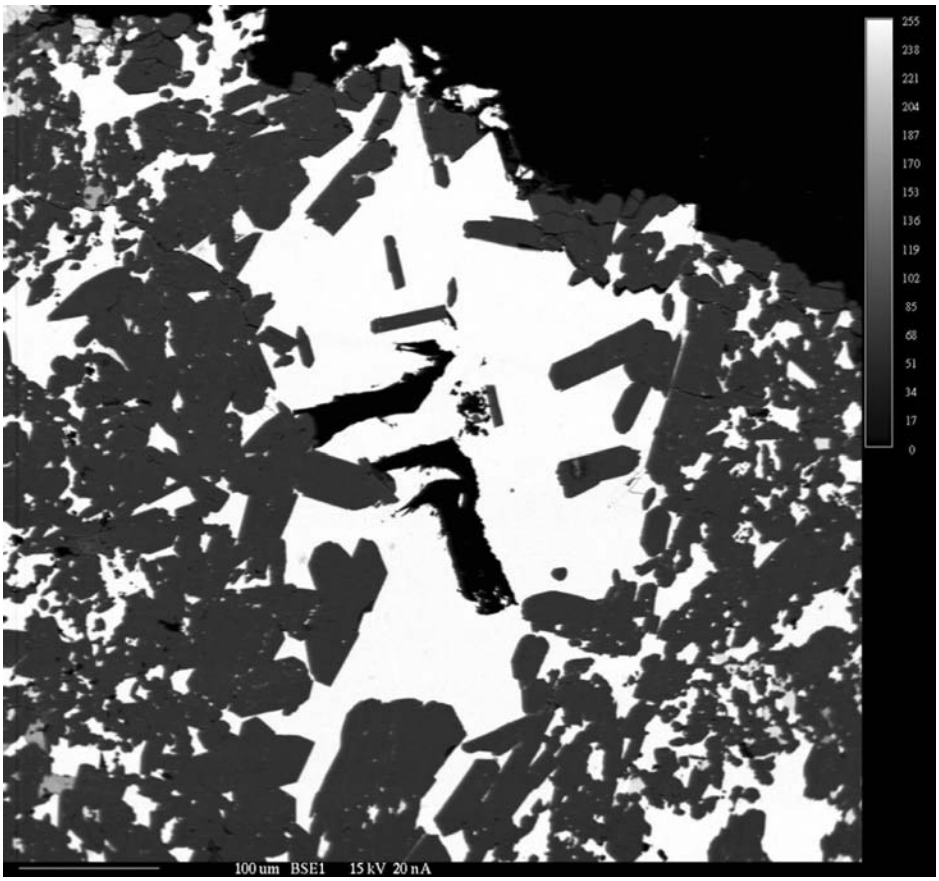

Fig. 4. Photomicrograph of interstitial graphite adjacent to a melt pocket (fine-grained, anhedral black phase) and subhedral graphite laths (black) enclosed by Fe, Ni-metal (bright phase) of a melt pocket in Grein 002 (field of view is ~600 × 700 μm). Rubin (1997b) interprets euhedral graphite in EL chondrites as impact melt products. Its close association with the melt pockets in Grein 002 is consistent with this hypothesis. The fine-grained, anhedral interstitial occurrences of graphite in Grein 002 appear to be of primary origin.

Scott 1997), Grein 002 largely preserved its chondritic character and exhibits no conclusive sign of brecciation or total melting. The event that caused melting in Grein 002 was only locally effective. Yet, impact appears to be the only possible trigger. Shock waves are known to be heterogeneously distributed throughout a rock composed of different minerals and components, which cause variations in shock impedance (Stöffler et al. 1991). This effect is most pronounced at metal-silicate and metal-pore space interfaces. Metal-silicate interfaces are certainly common in Grein 002.

The greater amount of ferrosilite in euhedral enstatite of Grein 002 (as opposed to the ferrosilite content of anhedral enstatite) suggests crystallization under slightly less reducing conditions. The change in oxygen fugacity may reflect the prevailing level in the enstatite chondrite region at the time of the pocket-forming impact event. Alternatively, it may indicate "contamination" from the impactor, as demonstrated in the case of the Galim breccia (Rubin 1997a).

The Metal Phase

Grein 002 contains both kamacite and taenite. The Si content of kamacite does not exceed 1 wt% and, therefore, clearly qualifies for an EL classification (Tables 3a and 3b). Taenite is considered to be a rare metal phase in enstatite chondrites (Kong et al. 1997). Interestingly, our microprobe observations reveal that it contributes significantly to the total amount of metal in Grein 002. Its relatively high abundance is also reflected in the bulk Ni concentration (Table 1). This deviation may be simply another example for the well-known heterogeneity of enstatite chondrite material, or it may imply unusually rapid cooling of the Grein 002 area before most of the taenite was transformed into kamacite (see Romig and Goldstein 1991; Kong and Ebihara 1996). Sudden rapid cooling, however, can only be explained by impact-induced excavation or exposition and is inconsistent with other mineralogical evidence testifying to a more complex history of Grein 002.

Phosphorus trapped in the Fe-Ni phase of the melt pockets exsolved as schreibersite. It usually forms inclusions of up to 50 μm across in the coarse Fe-Ni patches. We found only one crystal that coexists with troilite. This latter grain reveals a significantly higher Ni content (33 wt%) than the average value of 23.1 wt%. Exsolution of schreibersite took place upon slow cooling at subsolidus temperatures (Blau and

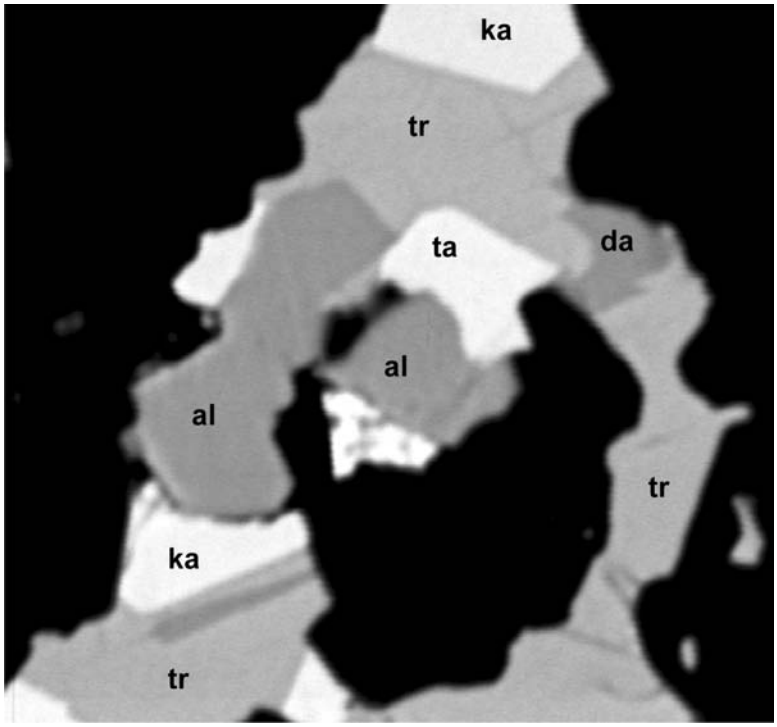

Fig. 5. Photomicrograph of one of the two tiny copper grains (center) that we detected in Grein 002 (field of view is ~40 μm across). In this case, it is attached to a primary interstitial sulfide assemblage including alabandite (al), troilite (tr), daubreelite (da), taenite (ta), and kamacite (ka).

Table 2. Chemical composition of transparent mineral phases in Grein 002 (av. wt%).[a]

	Enstatite[b]	Diopside[c]	Feldspar[d]	Forsterite[e]	Oldhamite	Sinoite
Si	27.8 ± 0.2	25.8 ± 0.3	31.0 ± 1.0	20.1 ± 0.1	0.12 ± 0.04	57.0 ± 0.6
Al	0.08 ± 0.01	0.22 ± 0.01	11.3 ± 0.5	b.d.	–	–
Ca	0.54 ± 0.06	17.2 ± 0.3	1.98 ± 0.75	0.05 ± 0.03	53.0 ± 0.4	–
Na	b.d.	0.13 ± 0.02	7.07 ± 0.26	b.d.	–	–
Mg	24.4 ± 0.1	12.1 ± 0.2	0.04 ± 0.03	34.8 ± 0.2	0.16 ± 0.05	–
Fe	0.37 ± 0.24[f]	0.21 ± 0.11	0.30 ± 0.23	0.31 ± 0.12	0.58 ± 0.31	–
K	b.d.	b.d.	0.64 ± 0.14	b.d.	–	–
Mn	–	–	–	–	0.95 ± 0.09	–
S	–	–	–	–	42.4 ± 0.2	–
N	–	–	–	–	–	28.2 ± 0.5
O	48.1 ± 0.2	44.5 ± 0.4	48.9 ± 0.6	45.9 ± 0.2	–	16.4 ± 0.5
Total	101.2 ± 0.5	100.2 ± 0.7	101.1 ± 1.0	101.1 ± 0.4	97.3 ± 0.2	101.5 ± 0.4
n	50	20	14	4	10	7

[a]b.d. = below detection limits; n = number of analyses.
[b]$En_{98.0 \pm 0.4}Fs_{0.65 \pm 0.42}Wo_{1.31 \pm 0.15}$.
[c]$En_{53.6 \pm 0.7}Wo_{46.0 \pm 0.8}Fs_{0.39 \pm 0.21}$.
[d]$Ab_{83.0 \pm 2.9}An_{12.1 \pm 3.8}Or_{4.87 \pm 1.14}$.
[e]$Fo_{99.6 \pm 0.2}Fa_{0.38 \pm 0.15}$.
[f]Average of anhedral (<0.5 wt% Fe) and euhedral enstatite (>0.5 wt% Fe).

Goldstein 1975). Temperatures must have been at least as high as 850 °C to induce subsolidus nucleation and growth of the phosphide (Clarke and Goldstein 1978). While the remaining kamacite now exhibits a relatively flat Ni distribution pattern, schreibersite appears to reveal a trend of increasing Ni abundances toward its center (Fig. 6). Ni abundances also vary considerably from grain to grain and, thus, support a grouping with the EL chondrites (Ni values of schreibersite in EH chondrites tend to be rather uniform; see Lin and El Goresy 2002; Tables 3a and 3b).

Sulfides

Sulfides in enstatite chondrites are an important component and usually exhibit considerable diversity. In Grein

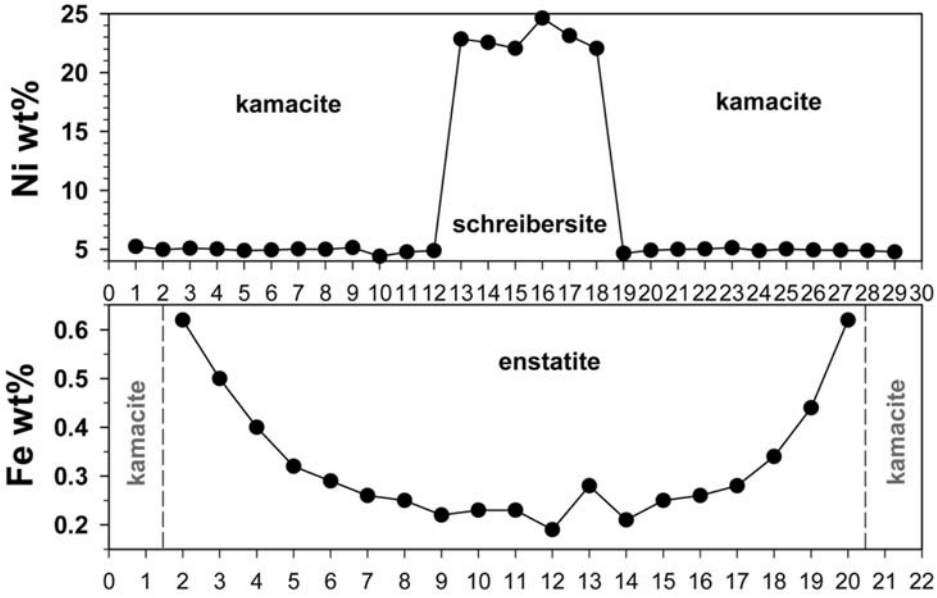

Fig. 6. Zoning patterns in euhedral enstatite and coarse kamacite of Grein 002. The euhedral enstatite crystals that are associated with coarse Fe, Ni-metal patches (melt pockets) exhibit increasing Fe concentrations from their centers to the rims. Mg abundances stay constant. The Fe zoning was most likely established when the melt pockets were formed (normal igneous zoning). In addition, the ferrosilite content of these euhedral pyroxenes is slightly higher than that of the anhedral, fine-grained enstatite, suggesting an increase in oxygen fugacity. The coarse kamacite patches show relatively flat Ni distribution patterns and sometimes contain exsolved schreibersite crystals with variable Ni concentrations. The analysis points in kamacite and enstatite are 10 and 5 μm apart, respectively.

002, we identified ubiquitous troilite, oldhamite, minor ferroan alabandite, daubreelite, and an Fe-dominated Zn-sulfide with exceptionally high Mn contents (Tables 3a and 3b). This latter phase shows a cubic structure and is most likely the Fe-rich equivalent of sphalerite (Zn, Fe-sulfide). Alabandite is diagnostic of EL chondrites and is nonexistent in EH chondrites (Fig. 7). With respect to its chemical composition, it is interesting to note that this sulfide displays a normal zoning trend with decreasing Fe concentrations from the center toward troilite (Fig. 8; e.g., Ehlers and El Goresy 1988). Normal zoning in niningerite (the Mg, Fe, Mn-sulfide found in EH chondrites; Fig. 7) is indicative of simple syn- or postaccretionary cooling. In contrast to this setting, reverse zoning with increasing Fe abundances toward troilite is interpreted as a secondary feature established by subsequent parent body metamorphism. Elevated temperatures after parent body formation would have induced the diffusion of Fe from troilite into niningerite (Ehlers and El Goresy 1988). Thus, the systematic decrease of Fe in alabandite suggests that the Grein 002 region escaped secondary thermal alteration. Evidently, textural and compositional parameters like the resorption and deformation of chondrules and the equilibrated nature of enstatite and diopside are inconsistent with this interpretation. The discrepancy suggests that diffusion kinematics between Mn-rich alabandite and troilite are different from those observed for the niningerite-troilite assemblage.

A systematic decrease of Fe concentrations toward troilite is also observed in the Fe-dominated equivalent of sphalerite (Fig. 8). In this case, the trend has been attributed to Fe diffusion from sphalerite into troilite due to parent body metamorphism (El Goresy and Ehlers 1989). This finding is concordant with the equilibrated character of Grein 002. In addition, evidence for relatively slow subsolidus cooling is established in the exsolution of daubreelite from troilite (El Goresy and Kullerud 1967).

Sphalerite is known to be a prominent Zn, Fe-sulfide in enstatite chondrites and exhibits a broad range of Mn concentrations (Nagel et al. 1989; Lin and El Goresy 2002). It also displays very variable Fe contents (e.g., Lin and El Goresy 2002). In a strict sense, according to the definitions given by the International Mineralogical Association (Nickel 1992), we detected a cubic Fe-dominated Zn-sulfide but no sphalerite in Grein 002. Its chemical composition varies between $(Fe_{0.45}Zn_{0.33}Mn_{0.20})S_{1.02}$ and $(Fe_{0.41}Zn_{0.35}Mn_{0.22})S_{1.02}$ (Tables 3a and 3b). An unnamed mineral of similar composition has been reported by Buseck and Holdsworth (1972). The Mn abundances of this sulfide are comparable to those reported for MAC 88136 yielding the highest MnS content in sphalerite observed so far (Fig. 9). Nagel et al. (1989) postulated a direct relation between the MnS content of sphalerite (and niningerite in EH chondrites) and the oxygen fugacity at the time of its crystallization. Apparently, increasing MnS values indicate more reducing conditions, suggesting an especially low oxygen fugacity in the formation environment of the Grein 002 parent rock (probably lower than the approximate range of $\log fO_2$ –20 to –17 estimated for the Abee impact melt breccia [Rubin 1997c]).

Table 3a. Chemical composition of opaque mineral phases in Grein 002 determined in Tucson (av. wt%).[a]

	Kamacite	Taenite	Troilite	Alabandite	Fe, Zn-sulfide	Daubreelite	Schreibersite	Osbornite
Fe	92.8 ± 1.1	84.0 ± 3.3	60.2 ± 0.8	12.9 ± 1.3	27.5 ± 0.9	17.4 ± 0.8	61.3 ± 2.9	1.26 ± 0.5
Ni	5.20 ± 0.41	14.1 ± 2.4	0.11 ± 0.14	b.d.	b.d.	b.d.	23.1 ± 3.2	b.d.
Si	0.54 ± 0.17	0.77 ± 0.58	0.06 ± 0.02	0.13 ± 0.10	0.14 ± 0.16	0.18 ± 0.10	0.07 ± 0.01	0.17 ± 0.06
Mg	b.d.	b.d.	b.d.	2.45 ± 0.56	0.19 ± 0.07	b.d.	b.d.	b.d.
Mn	b.d.	0.07 ± 0.09	0.15 ± 0.12	44.6 ± 1.8	11.5 ± 1.1	1.64 ± 0.27	b.d.	b.d.
Cr	0.19 ± 0.07	0.15 ± 0.07	0.92 ± 0.42	0.12 ± 0.08	b.d.	34.5 ± 0.7	b.d.	0.31 ± 0.09
Zn	b.d.	0.14 ± 0.09	0.10 ± 0.03	b.d.	24.0 ± 1.2	0.29 ± 0.15	b.d.	b.d.
Ti	b.d.	b.d.	0.42 ± 0.07	b.d.	b.d.	0.15 ± 0.08	b.d.	72.9 ± 0.3
Cu	b.d.	b.d.	b.d.	b.d.	b.d.	0.20 ± 0.06	b.d.	b.d.
Co	0.35 ± 0.07	0.15 ± 0.05	b.d.	b.d.	b.d.	b.d.	0.08 ± 0.05	b.d.
S	b.d.	b.d.	36.6 ± 0.4	37.8 ± 0.3	35.1 ± 0.2	44.1 ± 0.3	0.09 ± 0.01	b.d.
P	0.08 ± 0.04	b.d.	b.d.	b.d.	b.d.	b.d.	15.9 ± 0.2	b.d.
Ca	b.d.	b.d.	b.d.	0.20 ± 0.05	b.d.	b.d.	b.d.	b.d.
N	–	–	–	–	–	–	–	23.0 ± 0.6
Total	99.2 ± 0.8	99.3 ± 0.9	98.5 ± 0.4	98.4 ± 0.3	98.9 ± 0.6	98.3 ± 0.3	100.6 ± 0.8	97.9 ± 1.4
n	29	9	24	29	23	12	11	2

[a]b.d. = below detection limits; n = number of analyses.

Table 3b. Chemical composition of opaque mineral phases in Grein 002 determined in Hamburg (av. wt%).[a]

	Kamacite	Troilite	Alabandite	Fe, Zn-sulfide	Daubreelite	Schreibersite	Osbornite
Fe	94.5 ± 0.8	60.6 ± 0.3	12.9 ± 1.4	26.2 ± 1.0	17.0 ± 0.3	60.3 ± 2.2	1.97
Ni	4.47 ± 0.33	0.07 ± 0.01	0.04 ± 0.03	0.05 ± 0.02	0.15 ± 0.14	24.8 ± 2.2	–
Si	0.46 ± 0.06	–	–	–	–	0.04 ± 0.01	–
Mg	–	b.d.	2.67 ± 0.88	0.23 ± 0.06	0.07 ± 0.08	–	–
Mn	–	0.11 ± 0.06	44.9 ± 1.3	11.7 ± 0.9	2.45 ± 0.55	–	–
Cr	–	0.71 ± 0.06	0.16 ± 0.17	–	34.5 ± 0.2	–	–
Zn	–	0.08 ± 0.11	0.12 ± 0.14	24.6 ± 0.9	0.12 ± 0.15	–	–
Ti	–	0.29 ± 0.14	0.03 ± 0.06	–	0.16 ± 0.11	–	73.5
V	–	0.04 ± 0.01	–	–	b.d.	–	–
Co	0.42 ± 0.02	0.04 ± 0.04	–	–	b.d.	0.08 ± 0.01	–
S	0.01 ± 0.01	37.0 ± 0.1	38.4 ± 0.6	35.5 ± 0.1	44.4 ± 0.3	0.09 ± 0.01	–
P	–	–	–	–	-	13.2 ± 0.4	–
Ca	0.01 ± 0.01	0.06 ± 0.03	0.21 ± 0.07	-	0.08 ± 0.09	0.07 ± 0.07	–
N	–	–	–	–	–	–	22.2
Total	99.7 ± 1.2	98.9 ± 0.2	99.7 ± 0.7	98.3 ± 0.4	98.8 ± 0.2	98.4 0.8	97.7
n	6	4	10	6	3	4	1

[a]b.d. = delow detection limits; n = number of analyses.

Shock Effects

Stöffler et al. (1991) described shock-induced melt pockets and dikes in ordinary chondrites as being associated with opaque shock veins. According to those authors, the opaque veins form as frictional melts before the emplacement of the intrusive melt pockets and dikes during the pressure release phase of the rock. Melt pockets are also counted among whole rock effects of shock in enstatite chondrites (Rubin et al. 1997). Such pockets, however, have been solely observed in association with opaque shock veins, mosaicism in pyroxene, and maskelynitization, i.e., within rocks reflecting a much higher general shock stage (S5 and 6). With the exception of a single diffuse opaque vein, none of the phenomena listed above can be confirmed for Grein 002. Grein 002 shows signs of only weak shock metamorphism in conjunction with melt pockets.

In an attempt to reconstruct the sequence of events, we may assume that the formation of the melt pockets and possibly other shock features predated the metamorphic event that converted Grein 002 into a type 4–5 enstatite chondrite. In this case, the thermal alteration certainly induced recrystallization of maskelynite, which readily responds to an increase in temperature (Ostertag and Stöffler 1982). Recrystallized maskelynite is polycrystalline. Plagioclase in Grein 002, however, is anhedral and monocrystalline, therefore excluding the pre-existence of maskelynite. Provided that the thermal event lasted long enough, it may also have annealed features like mosaicism and fractures in

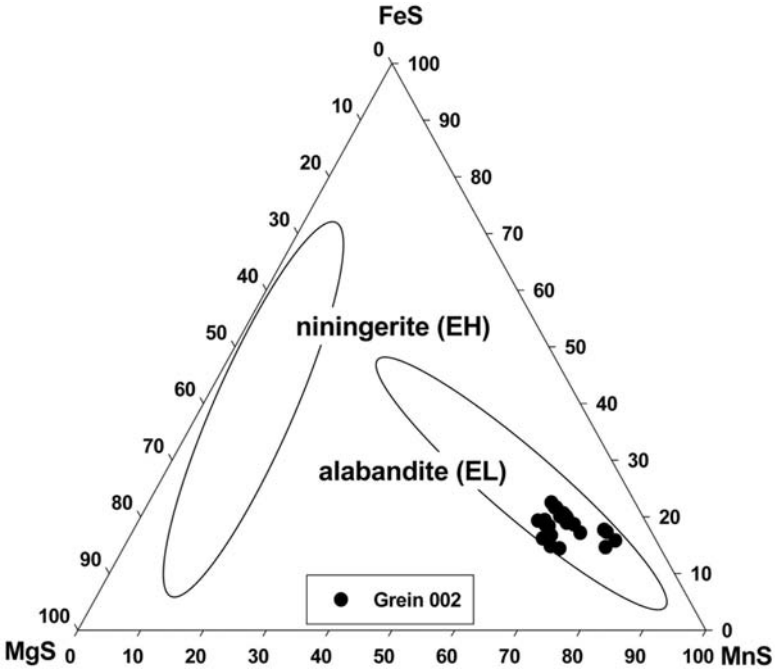

Fig. 7. Composition of the Mg, Mn, Fe-sulfide in Grein 002. While EH chondrites contain a more Mg-rich variant of this sulfide (niningerite), the Mn-rich subtype (ferroan alabandite) is diagnostic of EL chondrites.

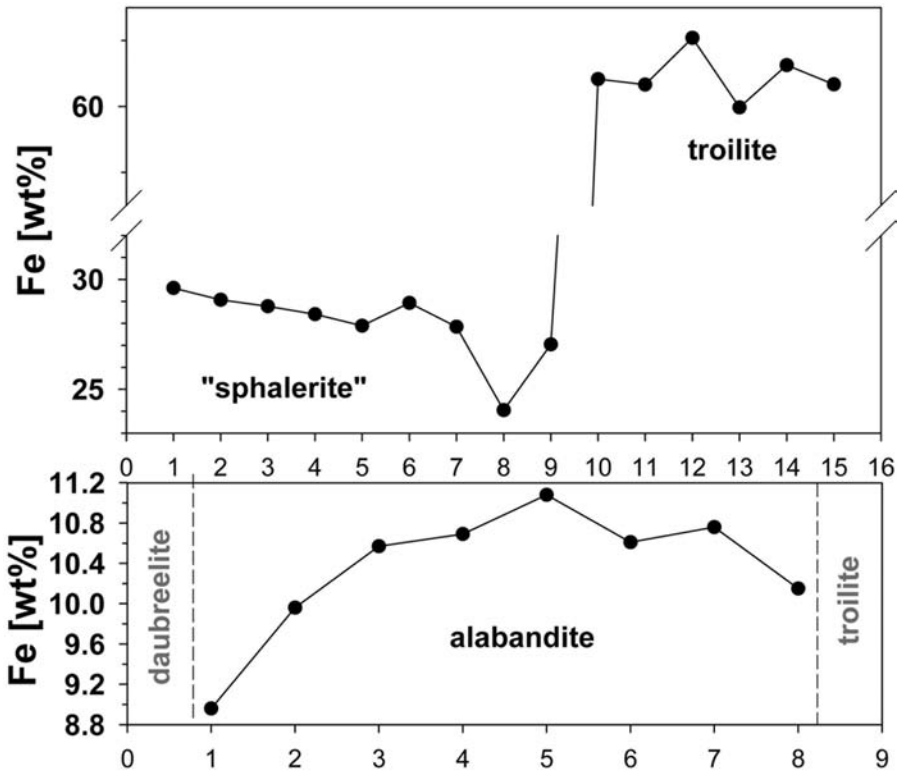

Fig. 8. Zoning patterns observed in alabandite and the Fe, Zn-sulfide (Fe-dominated equivalent of sphalerite) of Grein 002. Both sulfides display normal zoning with decreasing Fe concentrations toward adjacent troilite. Normal zoning in sphalerite implies significant thermal alteration that happened on the parent body (secondary metamorphism; El Goresy and Ehlers 1989). The zoning trend is consistent with textural and mineralogical findings. We assume that the systematical distribution of Fe in alabandite was established during the same thermal event. Zoning profiles were determined in 5 μm steps.

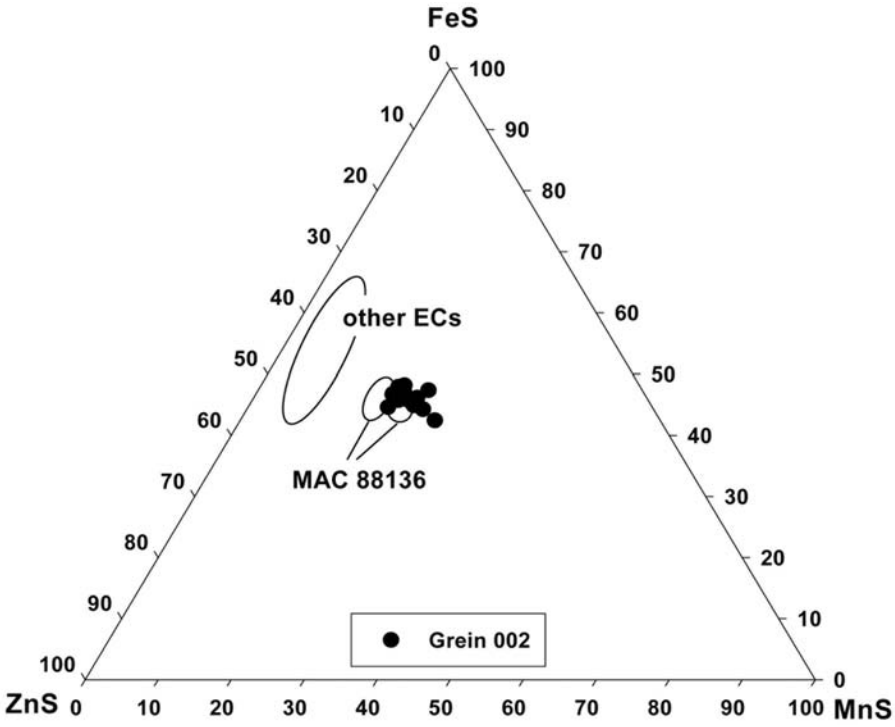

Fig. 9. Composition of the Fe, Zn, Mn-sulfide in Grein 002. We refer to this sulfide as the Fe-dominated equivalent of sphalerite. Sphalerite in enstatite chondrites is usually relatively Mn-poor (other ECs: data from Lin and El Goresy [2002]). So far, the sphalerite in the EL3 chondrite MAC 88136 has been known to show the highest MnS content (Nagel et al. 1989). The Fe, Zn-sulfide in Grein 002 reveals similarly high MnS values.

Table 4a. Reflectance data of selected mineral phases in Grein 002.[a]

λ nm	400	420	440	460	470	480	500	520	540	546	560	580	589	600	620	640	650	660	680	700
Schreibersite (VHN_{50} = 874–927)																				
R_1 (air)	44.0	43.9	43.7	43.3	43.0	42.8	43.3	44.0	44.6	44.9	45.3	46.5	47.0	47.4	48.6	49.5	50.0	50.2	51.6	52.9
R_2 (air)	45.0	45.0	45.5	45.8	45.9	45.9	46.2	47.0	47.7	47.9	48.4	49.4	50.0	50.3	51.4	52.2	52.7	53.1	54.1	55.2
R_1 (oil)	31.3	31.5	32.4	33.0	33.1	33.2	33.5	33.9	34.6	34.8	35.3	36.3	36.8	37.2	38.1	38.8	39.1	39.5	40.4	41.3
R_2 (oil)	31.7	31.9	33.0	33.6	33.6	33.7	33.8	34.4	35.1	35.2	35.7	36.8	37.2	37.6	38.7	39.4	39.8	40.2	41.1	42.1
Troilite (VHN_{50} = 306–358)																				
R_1 (air)	30.6	30.8	30.1	29.6	29.6	29.4	29.6	30.6	31.7	31.8	32.5	33.4	34.0	34.5	35.7	37.1	37.5	37.9	39.4	40.7
R_2 (air)	32.0	32.1	32.1	32.3	32.5	32.8	33.3	34.3	35.5	35.8	36.3	37.0	37.5	38.1	39.1	40.3	40.8	40.9	42.1	43.1
R_1 (oil)	15.8	15.9	16.8	17.7	18.2	18.5	19.2	20.1	21.2	21.5	22.1	23.1	24.0	24.2	25.2	26.1	26.5	26.9	27.7	28.6
R_2 (oil)	16.9	16.9	17.7	18.7	19.2	19.8	20.5	21.4	22.4	22.8	2.4	24.4	25.0	25.5	26.4	27.3	27.7	28.2	28.8	29.6
Alabandite (VHN_{50} = 271–289)																				
R (air)	28.6	27.2	26.4	25.2	25.0	24.3	23.7	23.5	23.2	23.1	22.9	22.8	22.8	22.6	22.6	22.6	22.6	22.6	22.9	23.1
R (oil)	12.2	11.5	11.0	11.0	10.5	10.3	10.1	10.1	9.9	9.9	9.9	9.8	9.8	9.7	9.5	9.5	9.5	9.5	9.5	9.5
Kamacite (VHN_{50} = 214–251)																				
R (air)	52.9	54.1	55.3	56.5	57.0	57.6	58.0	57.9	57.8	58.0	58.0	58.3	58.3	58.4	58.6	58.6	58.6	58.7	58.8	59.0
R (oil)	39.4	41.1	41.6	41.2	40.3	39.8	39.5	39.4	39.4	39.4	39.4	40.1	40.1	40.4	41.1	41.5	41.7	42.1	42.9	43.7
Osbornite (VHN_{50} = ~150)																				
R (air)	39.2	34.7	30.7	30.8	32.1	34.6	37.6	43.0	47.8	48.1	50.8	53.2	54.1	55.6	57.2	58.2	58.3	58.5	58.9	59.8
R (oil)	24.2	20.0	17.4	17.0	17.5	18.9	21.3	25.6	30.3	31.0	33.7	36.8	37.9	40.1	42.8	45.2	45.8	46.4	47.9	49.0
Fe, Zn-sulfide[b]																				
R (air)	23.8	23.0	22.1	20.9	20.3	19.7	19.0	18.8	18.4	18.2	18.1	18.0	17.9	17.9	17.9	17.9	17.9	18.0	18.1	18.3
R (oil)	8.1	8.0	7.4	6.7	6.4	6.1	5.8	5.7	5.6	5.6	5.5	5.5	5.5	5.4	5.4	5.4	5.4	5.4	5.5	5.6
Oldhamite (VHN_{50} = 237–265)																				
R (air)	12.5	12.3	12.0	11.8	11.7	11.6	11.5	11.5	11.5	11.5	11.5	11.5	11.5	11.5	11.5	11.5	11.5	11.5	11.6	11.7

[a]All values represent the average result of several (>5) measurements of central grain regions; VHN_{50} = Vickers micro hardness (see Analytical Techniques).
[b]Individual grains were too small to allow the determination of the VHN_{50} values.

Table 4b. Color values of selected mineral phases in Grein 002.[a]

C illuminant	x	y	Y %	Pe %	λ d
Schreibersite					
R_1 (air)	0.320	0.321	45.6	3.9	589
R_2 (air)	0.320	0.322	48.6	4.4	584
R_1 (oil)	0.323	0.325	35.5	5.9	584
R_2 (oil)	0.323	0.324	35.9	5.6	585
Troilite					
R_1 (air)	0.326	0.324	32.5	6.6	588
R_2 (air)	0.326	0.328	36.2	7.6	582
R_1 (oil)	0.341	0.341	22.0	15.1	581
R_2 (oil)	0.340	0.341	23.3	14.9	580
Alabandite					
R (air)	0.301	0.304	23.1	4.8	471
R (oil)	0.301	0.307	9.9	4.1	476
Kamacite					
R (air)	0.313	0.321	58.0	2.3	572
R (oil)	0.311	0.312	39.9	1.8	543
Osbornite					
R (air)	0.359	0.361	49.1	25.2	579
R (oil)	0.386	0.371	32.7	35.7	582
Fe, Zn-sulfide					
R (air)	0.297	0.298	18.4	6.9	469
R (oil)	0.292	0.288	5.6	10.2	466
Oldhamite					
R (air)	0.308	0.313	11.5	1.2	467

[a]All values represent the average result of several (>5) measurements of central grain regions.

enstatite. However, no signs of extensive recrystallization exist in Grein 002. Furthermore, igneous Fe zoning in the euhedral pyroxene crystals likely would have been annealed in the course of such a thermal regime.

If we assume metamorphism happened before the generation of the observed melt pockets, the question arises why Grein 002 displays no phenomena of severe or at least moderate shock. An impact capable of inducing local melting should also leave fingerprints like abundant opaque veins, mosaicism, fracturing, and possibly maskelynitization. On the other hand, it has been shown that "the onset and abundance of shock-induced localized melting strongly depends on the initial temperature of the sample" (e.g., Schmitt 2000). We could, therefore, speculate that Grein 002 was still in the stage of thermal metamorphism when it was hit by a shock wave.

Despite these obvious uncertainties, impact-induced shock melting of Grein 002 appears to be the most likely scenario with respect to the formation of the confined melt areas. Possibly, the abundant metal grains absorbed most of the heat produced by friction prompted by the shock pulse. Subsequently, during the stage of rock dilatation, part of the Fe-Ni phase was converted into liquids and consolidated as the observed large metal patches. The locally increased temperatures also initiated melting of pyroxene leading to euhedral enstatite grains protruding the molten metal regions. The relatively high surface energy and high surface energy anisotropy of enstatite crystals (e.g., Spry 1969) facilitated euhedral growth. Experimental studies yielded pyroxene growth rates in a multi-component system of ~1.2×10^{-4} cm/s at temperatures 20° below the liquidus (e.g., Dowty 1980). Another study of crystallization processes in an artificial magma determined minimum growth rates of 10^{-7} cm/s in the center of the melt (Dunbar et al. 1995). Euhedral enstatite in Grein 002 is up to ~200 μm long, suggesting that the largest crystals needed roughly 1.5 to 1500 sec to develop. The latter value is based on the scenario described by Dunbar et al. (1995) and involves relatively slow cooling (in the center of a melt body). Thus, it is most likely too high with respect to Grein 002. Evaluations of the thermal histories of shock-metamorphosed ordinary chondrites inferred first stage cooling rates (thermal equilibration of cold clasts and impact melt) in the order of <1 °C/s for most cases (Kring et al. 1996). Obviously, the cooling rate depends on the melt to clast ratio. The abundance and size of melt pockets in Grein 002 vary significantly (from sub-mm to ~1 cm) but approximately account for 20–30 vol%. An impact melt sheet consisting of 61 vol% clasts and 39 vol% melt with an initial melt temperature of 1600 °C has been estimated to cool by ~700 °C in 10 sec. Thereafter, the cooling rate decreases substantially (Onorato et al. 1978). The estimated melt/clast ratio in Grein 002 implies that melt pockets and surrounding host rock may have thermally equilibrated with a similar or somewhat higher rate. Overall, the data seem to suggest that the growth of euhedral enstatite with crystal sizes of ≤200 μm within tens of seconds is feasible.

Rubin (1997b, c) proposed that sinoite and euhedral graphite in enstatite chondrites may have formed via crystallization from an impact melt. Grein 002 contains a small amount of euhedral sinoite grains (~1 vol%) as well as a few graphite laths (anhedral and euhedral graphite amount to ~1.5 vol%). The graphite laths (Fig. 4) tend to be in close spatial relationship to the melt pockets and, hence, support Rubin's hypothesis. Sinoite in Grein 002, however, is heterogeneously distributed. We found needle-shaped crystals embedded in some coarse kamacite patches as well as euhedral crystals seemingly uncorrelated to the areas of impact melting.

INAA Data Including Bulk N and C Concentrations

Previous surveys of the bulk chemical properties of enstatite chondrites have shown that chemical fractionation processes in the formation region of this meteorite class differed from those observed for ordinary chondrites (e.g., Kallemeyn and Wasson 1986; Wasson and Kallemeyn 1988; Kong et al. 1997). In particular, typically lithophile elements are known to preferentially partition into sulfides, indicating highly oxygen deficient and sulfur dominated formation conditions. In addition, reactions that are usually volatility-

controlled appear to have followed different rules in the enstatite chondrite area. For instance, Se in EHs and Au in both EHs and ELs are enriched above the CI level relative to the major elements Mg and Co, in spite of their relatively low condensation temperatures. K and Na concentrations also exceed expected levels (Wasson and Kallemeyn 1988). In addition, Ni, Co, and Fe in EL chondrites may have displayed volatile rather than refractory behavior (Kong et al. 1997).

Lithophile Elements

Fig. 10 illustrates the concentrations of selected lithophile elements normalized to CI abundances and Si of EH and EL chondrites on one hand and Grein 002 on the other. In general, refractory lithophile elements exhibit subchondritic abundances for all enstatite chondrites. The only difference between EH and EL chondrites is a slight La enrichment in the former subgroup. Moderately volatile elements reveal more pronounced differences between EHs and ELs. The principal trends for EL chondrites are decreasing concentrations from Si to Mn and relative enrichments in K and Na. K and Na in EHs display slightly higher abundances than in ELs, while Mn is clearly more abundant. Finally, Zn in EH chondrites is depleted as expected (~0.5 × CI) but strongly subchondritic in ELs (~0.03 × CI).

Grein 002 displays relative abundances of refractory lithophile elements very similar to those of EL chondrites, including a diagnostic depletion of La. Among the moderately volatile lithophiles of Grein 002 plotted in Fig. 10, almost all elements nicely follow the trend established for EL chondrites. The only exception is Zn, which has been detected in a concentration nearly 10× higher than the average. Its major host phase is the Fe, Zn-sulfide. Based on the high Zn abundance, the sulfide appears to be present in a modal amount close to that reported for most EH chondrites. Considering the observed compositional heterogeneity of enstatite chondrites in general, this might well be the case.

Not shown in Fig. 10 but displayed in Table 1, the bulk splits of Grein 002 analyzed in Tucson, Arizona, exhibit slightly enriched REE compared to the Mainz samples. The deviation might be explained by a small admixture of fine-grained material similar to the <45 micron fraction analyzed in the EL6 chondrite Pillistfer (Lavrentjeva and Lyul 2003). The enrichment may result from a different sampling of fine-grained oldhamite (CaS). Indeed, Ca is slightly enriched in the Arizona samples, along with the REE. Kallemeyn and Wasson (1986) noted that there is more (trace element) variability between EL samples than for EH. The presence of an EH-type La/Sm ratio and the excess Zn in Grein 002 suggest that the fine-grained fraction may record heterogeneous nebular conditions before accretion of the EL parent body or bodies.

Siderophile Elements

Regarding the siderophile elements, EH chondrites are typically richer in opaque phases, particularly metal, than ELs and, therefore, exhibit higher elemental abundances (Fig. 11). Au is relatively enriched in both ELs and EHs, while Ga and

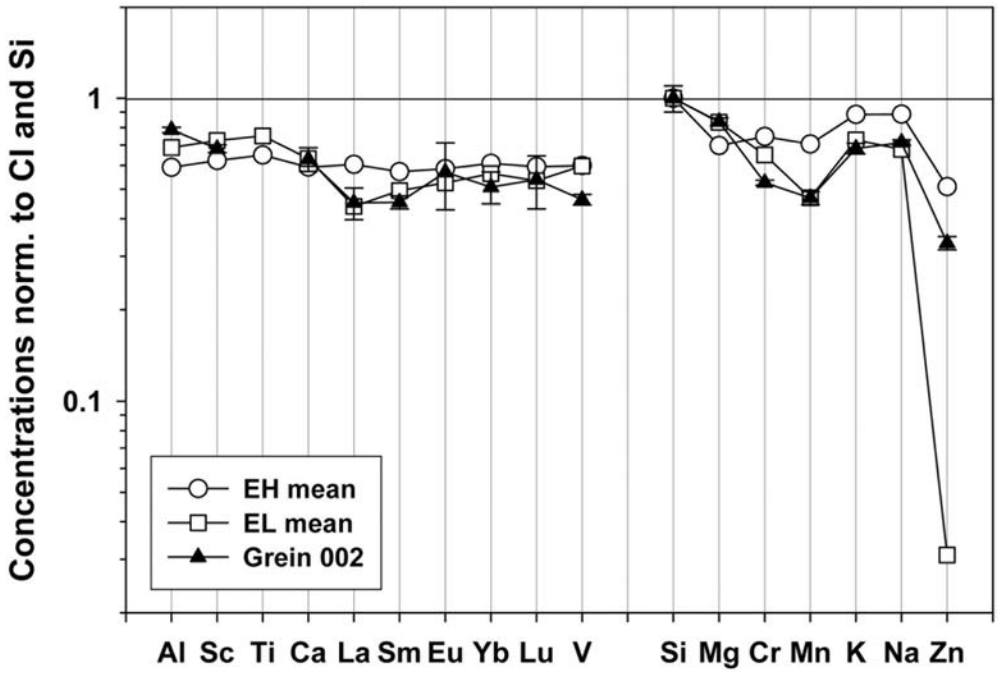

Fig. 10. Lithophile element concentrations normalized to CI abundances and Si in Grein 002. This graph illustrates the distribution patterns of refractory and moderately volatile lithophiles in EHs, ELs, and Grein 002. Overall, Grein 002 displays a typical EL chondritic signature. The only clear exception is Zn, showing an unusually high concentration. The major host phase of this element is the Fe, Zn-sulfide (the Fe-rich equivalent of sphalerite). Probably, the modal abundance of this type of sulfide in Grein 002 exceeds the average value.

Table 5. Noble gas data of Grein 002.[a]

	80.73 mg[b]	43.32 mg[c]	40.45 mg[c]	55.75 mg[c]	62.03 mg[d]	63.68 mg[d]	80.65 mg
^{3}He	53.1	59.5	58.5	54.5	58.3	58.3	57.5
^{4}He	1580	1170	1200	1310	1570	1250	945
^{20}Ne	12.6	11.0	10.9	10.8	11.7	11.3	–
^{21}Ne	9.36	9.8	9.24	9.16	9.91	9.97	–
^{22}Ne	11.3	11.5	10.9	10.8	11.7	11.8	–
^{36}Ar	126	33.6	55.5	74.8	54.9	43.3	52.5
^{38}Ar	25.0	7.69	11.7	15.5	11.5	9.27	11.4
^{40}Ar	7900	6070	6290	6560	7040	7020	4110
^{84}Kr	0.63	0.13	0.25	0.37	0.25	0.20	0.30
^{129}Xe	0.83	0.14	0.36	0.64	0.45	0.46	0.42
^{132}Xe	0.31	0.05	0.11	0.17	0.14	0.11	0.17
$^{3}He_c$	53.1	59.5	58.5	54.5	58.3	58.3	57.5
$^{21}Ne_c$	9.36	9.80	9.24	9.16	9.89	9.95	–
$^{38}Ar_c$	1.42	1.57	1.46	1.59	1.31	1.30	1.80
$(^{21}Ne/^{22}Ne)_c$	0.857	0.863	0.866	0.862	0.862	0.856	–
T_3	34.5	38.5	37.9	35.3	36.9	37.0	27.7
T_{21}	44.8	45.4	42.3	42.7	43.8	45.4	–
T_{38}	39.1	42.7	39.6	43.4	42.1	42.4	(19.7)
$^{4}He_r$	1310	816	852	981	1280	895	600
$^{36}Ar_{tr}$	125	32.6	54.6	73.8	54.0	42.4	51.3
T_4	3.84	2.88	2.97	3.28	3.76	3.08	2.26
T_{40}	4.65	4.39	4.42	4.46	4.53	4.53	4.00

[a]Gas concentrations in 10^{-8} cm^{3}STP/g; T_3, T_{21}, and T_{38} = cosmic ray exposure ages in Ma derived from $^{3}He_c$, $^{21}Ne_c$, and $^{38}Ar_c$, respectively; T_4 and T_{40} = gas retention ages calculated from $^{4}He_r$ and ^{40}Ar in Ga; indices: c = cosmogenic, r = radiogenic, tr = trapped.

[b]Data from Patzer and Schultz (2001).

[c]Data from Patzer and Schultz (unpublished); aliquants were part of a weathering experiment that revealed the effect of terrestrial alteration on the Ar, Kr, and Xe record of enstatite chondrites.

[d]Specimens consisting mainly of melt.

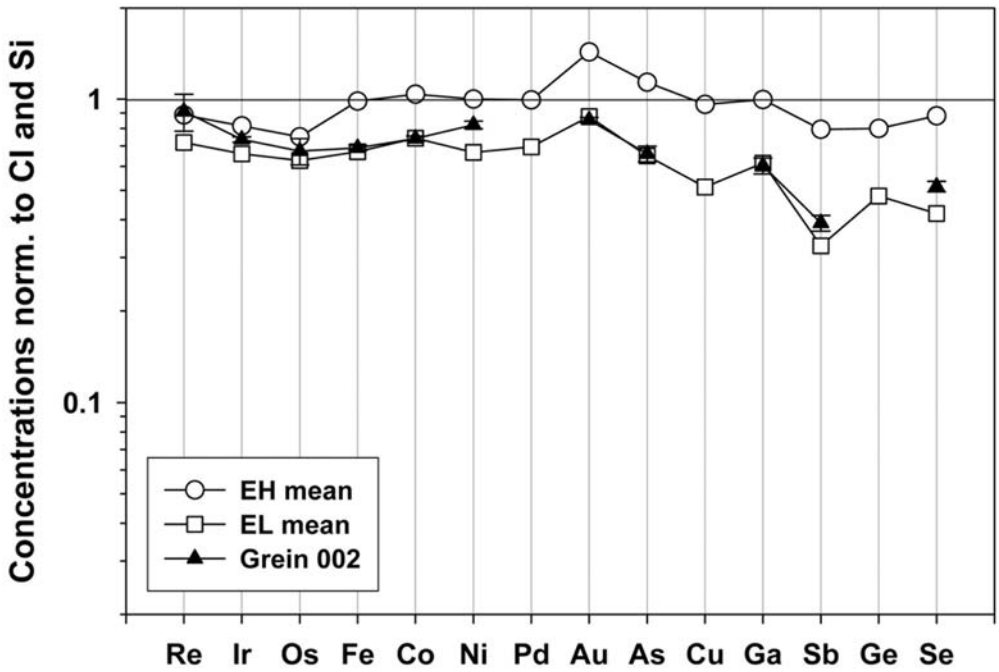

Fig. 11. Siderophile element concentrations normalized to CI abundances and Si in Grein 002. EH chondrites typically exhibit higher siderophile element concentrations than EL chondrites due to the higher modal abundance of metal. Again, the distribution pattern observed for Grein 002 closely resembles that of other EL chondrites. Only Ni deviates significantly from the average EL value and is relatively enriched. The discrepancy can be explained by the unusually high amount of taenite found in Grein 002.

Ge show relatively enhanced concentrations only in EL chondrites.

The pattern of siderophile elements in Grein 002 is similar to that of other EL chondrites and is consistent with the picture gathered from the lithophiles. Minor deviations include elevated concentrations of Ni and Se. The Ni abundance plots between the average EH and EL values and is likely enriched due to the unusually high amount of taenite detected in Grein 002 (see above). Selenium also reveals a slightly enriched concentration but still lies closer to the data point of ELs than to that of EHs (Fig. 11), possibly reflecting a slightly enriched content of troilite.

Overall, the INAA data support the suggestion that there were regional nebular heterogeneities, possibly over very short distances, within the EC source region (Kallemeyn and Wasson 1986). Kallemeyn and Wasson (1986) proposed that EL chondrites may have accreted to only 100 m-sized planetesimals (versus 10 km for EH) before experiencing metamorphism. The relatively small size of their parent bodies might explain the elemental variation observed between EL chondrites as well as that within a single, complex meteorite like Grein 002.

Carbon and Nitrogen Concentrations

The bulk contents of C and particularly N in enstatite chondrites are known to span a relatively wide array of values. The considerable heterogeneity can be explained by the variable distribution of their carriers. Both C and N are accommodated by minor mineral phases. C chiefly occurs as graphite, while N is bound in osbornite, sinoite, and possibly isostructurally as substitution for oxygen in silicate lattice sites (Baur 1972). No clear systematic relationships between the bulk concentrations of C and N and subgroup or petrologic type exist (e.g., Grady et al. 1986). It appears, however, that samples of the highest metamorphic grade (E6) yield the widest variation. Overall, carbon contents range from 0.15 to 0.70 wt%. Grein 002 contains ~0.55 wt% C (Table 1). No C data of other EL4–5 chondrites have been reported so far, but the value determined for Grein 002 falls into the upper range of quantities listed for EH4 and EH5 chondrites.

The N concentrations of enstatite chondrites vary between 0.01 and 0.1 wt% (Grady et al. 1986). For Grein 002, an average of 0.052 wt% N was measured (Seifert, personal communication; Table 1). Therefore, our sample shows an intermediate N content. This number appears to be inconsistent with the relatively high modal abundance of sinoite detected in one of the thin sections. The theoretical concentration of N calculated from 1.0 vol% sinoite (Si_2N_2O; applied densities: 2.82 g/cm^3 for sinoite and 4 g/cm^3 for the bulk rock) is 0.20 wt%. This value clearly exceeds the highest N concentration determined for any enstatite chondrite so far. We assume that the discrepancy results from a heterogeneous distribution of sinoite in the sample.

Noble Gas Inventory Including ^{26}Al Activity

We analyzed the noble gas record of two aliquants mainly consisting of melt pocket material as well as a bulk sample of Grein 002 (Table 5). In addition to these data, Table 5 lists the noble gas abundances and ratios of a previous analysis performed by Patzer and Schultz (2001, 2002). Overall, all data agree well or vary only as expected. No significant difference exists between the noble gas signatures of the melt samples and the bulk specimens. The similarity of concentrations and ratios suggests closed-system conditions for the melting/recrystallization event.

The Cosmogenic Component

While traveling through space, a meteoroid is exposed to cosmic irradiation. Galactic and solar cosmic rays trigger diverse nuclear reactions that allow the determination of cosmic ray exposure ages (CREA; e.g., Patzer and Schultz 2001, and references therein).

The Ne fraction of the noble gas inventory in Grein 002 is invariably dominated by the cosmogenic component as demonstrated by its isotopic composition (Table 5). The significance of cosmogenic ^{21}Ne as well as cosmogenic ^{3}He and ^{38}Ar for evaluating transfer times of meteorites has been well-established. The CREA calculated from cosmogenic ^{21}Ne (T_{21}) is generally considered to be the most reliable. ^{3}He exposure ages can be affected by diffusive loss due to solar heating on orbits with small perihelia (Hintenberger et al. 1966; Schultz and Weber 1995, 1997). Exposure ages based on cosmogenic ^{38}Ar (T_{38}), on the other hand, may yield higher uncertainties for samples with considerable amounts of trapped Ar. In addition, it has been shown that cosmogenic ^{38}Ar in stony meteorites is more likely to be altered by terrestrial weathering than ^{21}Ne or ^{3}He. This is particularly true for meteorites from hot deserts (Gibson and Bogard 1978; Scherer at al. 1994; Patzer and Schultz 2001). The latter concern is not applicable to Grein 002 (weathering degree W1). However, the amount of trapped heavy noble gases is high in this meteorite (see below). The uncertainty of T_{21} is estimated to be ~15%.

Patzer and Schultz (2001) report on the exposure age distribution of over 50 ECs. ECs exhibit a higher chemical heterogeneity than ordinary chondrites. Consequently, the T_{21} of these meteorites yields a higher uncertainty (~20%) that, as the authors conclude, tends to mask potential age clusters and, therefore, hampers the definition of major impact events. It seems, however, that EL6 chondrites typically display CREA >20 Ma, while EL4–5 chondrites yield T_{21} of ~1.7, 4.7, 21.8, and 44.6 Ma. The high end of this range at 44.6 Ma is marked by Grein 002 (Table 5). Only EL6 chondrites have been observed to yield similarly high CREA so far.

The comprehensive study of Patzer and Schultz (2001) also includes the first noble gas measurements and CREA determinations for Grein 002. They calculated a T_{21} of

44.1 Ma by applying chemical correction factors for the production rates of cosmogenic ^{3}He, ^{21}Ne, and ^{38}Ar that were based on the average composition of EL5 and EL6 chondrites (Kong et al. 1997). In this investigation, we used elemental data from our INAA analyses of Grein 002 and corrected the cosmogenic production rates accordingly. Based on the new chemical and noble gas data (Tables 1, 5), the T_{21} of Grein 002 averages 44.6 Ma. This is in very good agreement with the previously determined age.

The Radiogenic Component

The major fraction of ^{4}He and ^{40}Ar is of radiogenic provenance. In fact, we assume that the measured amount of ^{40}Ar was entirely derived from the radioactive decay of ^{40}K. Both radiogenic ^{4}He and ^{40}Ar are of interest when it comes to studying the thermal history of meteoritic matter. The concentrations of these rare gas isotopes in combination with the abundances of their parent nuclides (U + Th and K, respectively) can be translated into so-called gas retention ages that ideally indicate the last degassing of the rock. More often than not, however, the U/Th-He and the K-Ar "clocks" are not completely reset, and the resulting retention ages cannot be connected to specific events in the history of this material. This is particularly true for radiogenic ^{4}He, which is already mobilized at a few hundred degrees Celsius. By inference, the corresponding U/Th-He age is more readily modified (e.g., Anders 1964).

The higher susceptibility of He to diffusive loss at enhanced temperatures is also evident for Grein 002 (Table 5). As opposed to the U/Th-He age of only ~3.15 Ga, its K-Ar age of ~4.5 Ga appears to be almost undisturbed. Even though a substantial uncertainty may apply and the system has not been completely reset, the U/Th-He age most likely reflects partial degassing during the thermal event that followed accretion and induced equilibration.

The Trapped Component in the Heavy Noble Gases

Enstatite chondrites are known to display a bimodal trapped noble gas record: petrologic types 4 to 6 contain a diagnostic subsolar component, while type 3 samples reveal a Q-like signature (Q represents the noble gas pattern usually detected in ordinary and carbonaceous chondrites) suggesting distinct evolutionary paths for the primitive and metamorphosed enstatite chondrites (Patzer and Schultz 2002, and references therein).

In unweathered meteorites, ^{36}Ar as well as Kr and Xe are essentially primordial gases that were trapped during the formation of the parent material. From primordial rare gases, one may obtain information on the origin and early evolution of meteorites as they reflect compositional properties of meteoritic source regions (e.g., Swindle 1988; Ozima et al. 1998; Ott 2002).

Equilibrated ECs have been found to contain relatively high amounts of trapped noble gases despite their metamorphosed character (Crabb and Anders 1981; see also Patzer and Schultz 2002). Grein 002 also clearly exhibits this diagnostic subsolar pattern, confirming its classification as an equilibrated enstatite chondrite (Fig. 12; see also Patzer and

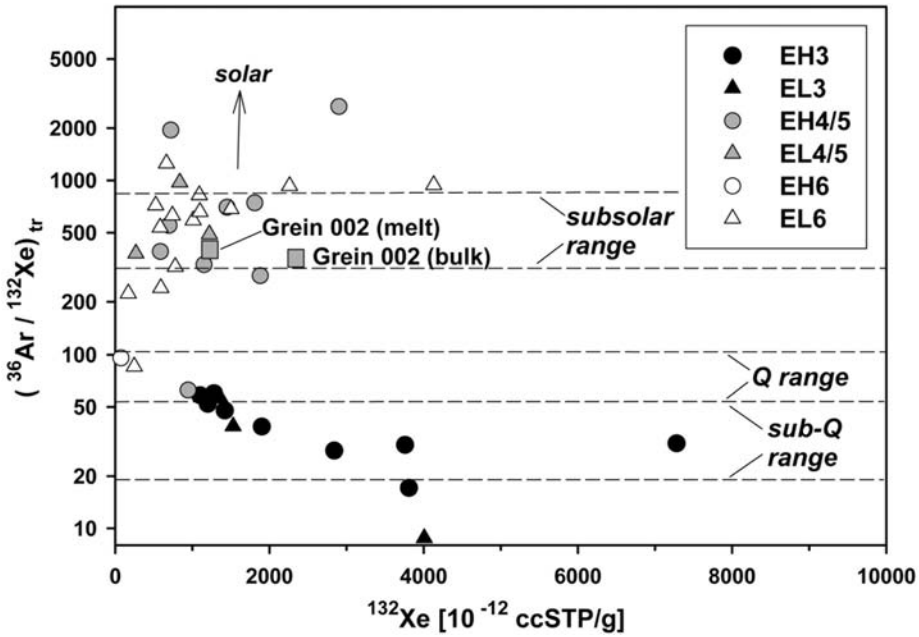

Fig. 12. Primordial heavy noble gases in Grein 002. Enstatite chondrites of petrologic type 3 are characterized by a primordial component with Q-like and sub-Q elemental ratios. The equilibrated ECs, on the other hand, show a diagnostic subsolar signature (Patzer and Schultz 2002). This component with relatively high Ar abundances is also present in Grein 002, confirming its classification as an equilibrated enstatite chondrite. The noble gas inventory of two specimens consisting mainly of melt material and that of a bulk sample of Grein 002 display basically identical noble gas records.

Schultz 2002). Unlike the case of ordinary chondrites, however, it is not possible to distinguish type 4, 5, and 6 ECs on the basis of absolute gas abundances.

In Fig. 13, the individual isotopic ratios $^{129}Xe/^{132}Xe$ have been plotted as a function of the trapped elemental ratios $^{84}Kr/^{132}Xe$. The diagram illustrates the influence of weathering on one hand and reveals the contribution of radiogenic ^{129}Xe, a decay product of radioactive ^{129}I ($T_{1/2}$ = 16 Ma), on the other. In the case of enstatite chondrites, the abundance of oxidized metal is not a reliable indicator of weathering due to its Si content. More sensitive evidence, however, can be expected from the record of the heavy noble gases Ar, Kr, and Xe (e.g., Scherer et al. 1994). Grein 002 seems to have experienced some terrestrial contamination of its noble gas inventory. A small contribution of terrestrial-like noble gases to the composition of the subsolar component has recently been suspected to be a characteristic feature of this particular rare gas pattern and may be derived from atmospheric gases (Busemann et al. 2003). The enstatite chondrite investigated by Busemann et al. (2003), however, was a fall. Therefore, we speculate that the terrestrial-like composition of the subsolar pattern may be a primary feature of this signature. This hypothesis is consistent with the noble gas data, the good preservation of oldhamite, and the radionuclide record (Schultz et al. 1998) of Grein 002. Provided that our suspicion can be confirmed, Fig. 13 would be inadequate for indicating alteration of samples that contain a subsolar noble gas component.

Fig. 13 also suggests the presence of excess ^{129}Xe. By inference, radioactive ^{129}I must still have been present when the Grein 002 material accreted. As opposed to ordinary chondrites, high concentrations of radiogenic ^{129}Xe are typical for enstatite chondrites (Crabb and Anders 1981).

^{26}Al Activity and Shielding Conditions

One additional method to obtain information on the shielding conditions experienced by a meteorite is provided by cosmogenic ^{26}Al. As for other cosmogenic nuclides, its production rate depends on chemical composition and sample depth (e.g., Heymann and Anders 1967; Vogt et al. 1990). The half-life of this radioactive cosmogenic isotope is 0.74 Ma ("long-lived").

The average saturated ^{26}Al content of H chondrites and ECs was found to be ~63 dpm/kg. Theoretical (calculated) values range around 60 dpm/kg (Heymann and Anders 1967). For Grein 002, an ^{26}Al activity of 49.7 ± 2.5 dpm/kg was determined by γ-γ-coincidence measurements (Altmaier, personal communication). This number is obviously lower than the expected saturated value. Undersaturation of ^{26}Al, however, can be excluded since the exposure age of Grein 002

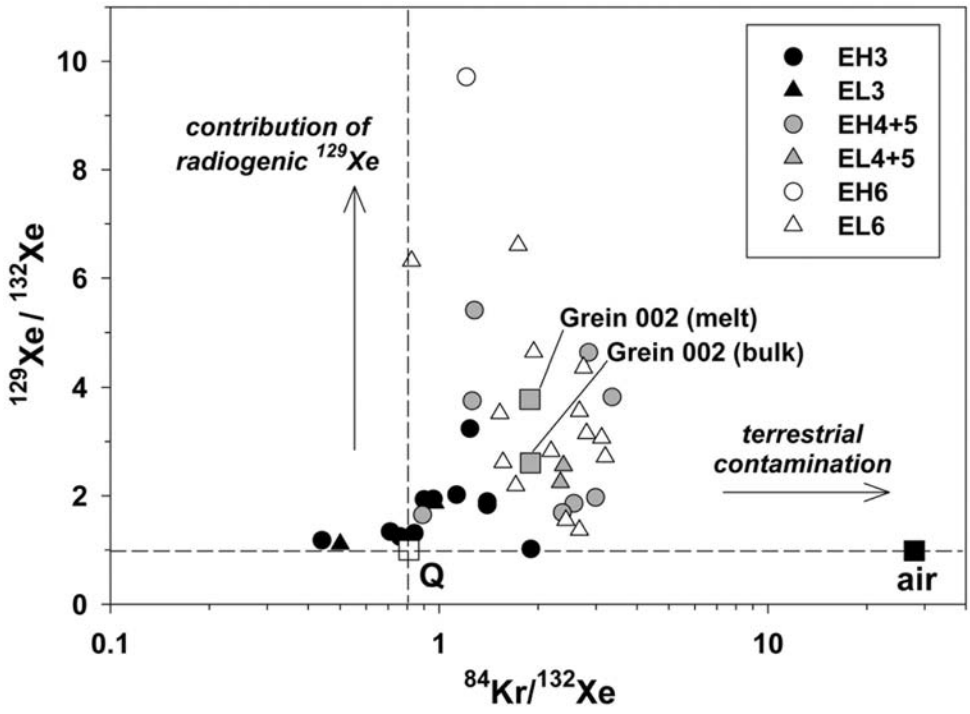

Fig. 13. This graph also depicts qualities of the trapped heavy noble gases in Grein 002. By plotting the trapped $^{84}Kr/^{132}Xe$ ratio as a function of the isotopic ratio $^{129}Xe/^{132}Xe$, the degree of terrestrial contamination as well as the contribution of radiogenic ^{129}Xe gas be assessed. Enstatite chondrites are known for bearing relatively high amounts of radiogenic ^{129}Xe (Crabb and Anders 1981). According to a recent study, the subsolar noble gas component of E4–6 chondrites appears to be generally affected by terrestrial alteration (Busemann et al. 2003). However, Grein 002 shows insignificant signs of weathering, suggesting that high $^{84}Kr/^{132}Xe$ ratios may be inherent to the subsolar signature rather than reflecting atmospheric alteration.

is ~45 Ma. Therefore, it seems likely that shielding slightly affected the production of ^{26}Al and, concequently, other cosmogenic nuclides. Particularly in ordinary chondrites, the cosmogenic ^{22}Ne/^{21}Ne ratio represents a reliable shielding indicator (e.g., Eugster 1988). Low ratios (<1.1) are generally indicative of deep shielding in large meteoroids, while high ratios (>1.2) portend less shielding either in a small body or near the surface of a larger meteoroid. Grein 002 yields a cosmogenic ^{22}Ne/^{21}Ne ratio of 1.18 that actually suggests "normal" shielding. For enstatite chondrites, however, the application of a shielding correction based on cosmogenic ^{22}Ne/^{21}Ne has proven to be problematic due to the differences in chemical composition (Patzer and Schultz 2001). Thus, we assume that shielding did contribute to the cosmogenic inventory, with the implication that Grein 002 originally was a larger meteoroid (>1 m in diameter).

SUMMARY AND CONCLUSIONS

Grein 002 exhibits an overall chondritic appearance with a diagnostic assemblage of EL chondritic minerals including ferroan alabandite, kamacite with very low Si concentrations, and schreibersite with variable Ni contents. On account of the often deformed or partially resorbed character of chondrules and the equilibrated compositions of enstatite and diopside, we concur with the original classification of Grein 002 as a type 4–5 EL chondrite (Grossman 1998).

As distinct from most other enstatite chondrites, Grein 002 contains an unusually high amount of taenite and a high MnS content in its Fe-dominated equivalent of sphalerite (cubic Fe, Zn-sulfide). The high taenite abundance appears to be an example of well-known compositional heterogeneity among enstatite chondrites. The MnS concentration of sphalerite has been proposed to be inversely related to the level of oxygen fugacity in the formation area of the parent rock (Nagel et al. 1989) and suggests that redox conditions also varied during the accretion of enstatite chondrites. In addition, slightly higher ferrosilite concentrations in secondary, euhedral enstatite appear to reveal a small increase of oxygen fugacity over time.

Euhedral enstatite in Grein 002 is associated with large patches of Fe, Ni-metal and lathy graphite. We interpret these relatively coarse-grained, sub-mm to cm-sized areas as melt pockets. Melting took place only as a localized process and was probably induced by shock. Puzzlingly, and in contrast to other enstatite melt breccias and rocks, shock phenomena other than the melt pockets indicate only weak shock metamorphism (S2). Possibly, Grein 002 was experiencing thermal metamorphism when the impact took place (see Schmitt 2000).

Another distinctive feature of Grein 002 is the occurrence of abundant diopside (~11.5 vol%), a silicate that is present but rare in unequilibrated enstatite chondrites and that is reported in low quantity for only one EL6 chondrite (EET 90102). The comparatively high amount of diopside in Grein 002 appears especially interesting in light of aubrite petrogenesis (see Fogel 1997; Floss et al. 2003).

Two sulfide phases (alabandite and the Fe, Zn-sulfide) display normal zoning trends. Normal zoning in sphalerite (Zn, Fe-sulfide) is believed to be established during parent body metamorphism (El Goresy and Ehlers 1989). We assume that normal zoning in the Fe-dominated equivalent of sphalerite also developed during a post-accretionary heating event. The regime of elevated temperatures was then followed by a period of slow subsolidus cooling that produced exsolution of daubreelite from troilite. The formation of melt pockets most likely can be assigned to a post-metamorphic impact event.

The chemical composition of Grein 002 is almost identical to that of average EL chondrites. Normalized to CI concentrations and the Si abundance of the sample, the lithophile elements reveal slightly subchondritic levels, including a diagnostic small enrichment of La. Only Zn is not as depleted as expected, suggesting a relatively high Fe, Zn-sulfide content. The concentrations of siderophile elements also mostly agree with typical EL values. The exceptions are enhanced Ni and Se abundances. While the high amount of Ni can be readily explained by the unusually high content of taenite, the enrichment in Se may reflect an above average abundance of troilite. Bulk concentrations of C and N fall into the known range.

The noble gas record of Grein 002 shows He and Ne dominated by the cosmogenic component. Ar, Kr, and Xe display a prominent primordial signature. The latter subsolar pattern is diagnostic of equilibrated enstatite chondrites. Grein 002 also contains the typical excess of radiogenic ^{129}Xe. Its ^{21}Ne cosmic ray exposure age is 44.6 Ma with an uncertainty of ~15%. So far, only EL6 chondrites have yielded ages >~34 Ma. U/Th-He and K-Ar gas retention ages have been calculated to be ~3.2 Ga and ~4.5 Ga, respectively. The former value may indicate that the U/Th-He system was modified (partial degassing of He) during the metamorphic event that equilibrated the Grein 002 parent region. The K-Ar age almost equals the canonical formation age and appears to be influenced by the high amount of primordial gases in Grein 002. Therefore, we consider it highly uncertain.

The ^{26}Al activity determined for Grein 002 turned out to be below the expected saturation level and suggests shielding of the sample in a slightly larger meteoroid (>1 m).

Acknowledgments–We would like to thank B. Spettel (Mainz) for processing and providing the first set of INAA data. We also appreciate the technical support of K. Domanik (Tucson) and B. Cornelisen (Hamburg) at the microprobe sessions. David Kring (Tucson) assisted with identifying shock phenomena and provided valuable ideas and conclusions regarding the thermal history of Grein 002. C and N concentrations were determined by R. Seifert (Hamburg). The

^{26}Al activity was provided by A. Altmaier (Köln). Constructive reviews by A. Rubin and the Associate Editor (K. Righter) as well as comments and suggestions of A. El Goresy clearly helped improve the original manuscript. The work by A. Patzer was supported by NASA grants NAG5/4944 (W. V. Boynton) and, during the review process, NAG5/12881 (D. A. Kring).

Editorial Handling—Dr. Kevin Righter

REFERENCES

Anders E. 1964. Origin, age, and composition of meteorites. *Space Science Reviews* 3:583–714.

Baur W. H. 1972. Occurrence of nitride nitrogen in silicate minerals. *Nature* 24:461–462.

Blau P. J. and Goldstein J. I. 1975. Investigation and simulation of metallic spherules from lunar soils. *Geochimica et Cosmochimica Acta* 39:305–324.

Brearley A. J. and Jones R. H. 1998. Chondritic meteorites. In *Planetary materials,* edited by Papike J. J., Washington D.C.: Mineralogical Society of America. pp. 3-01–3-370.

Busemann H., Eugster O., Baur H., and Wieler R. 2003. The ingredients of the "subsolar" noble gas component (abstract #1674). 34th Lunar and Planetary Science Conference. CD-ROM.

Buseck P. R. and Holdworth E. F. 1972. Mineralogy and petrology of the Yilmia enstatite chondrite. *Meteoritics* 7:429–447.

Clarke R. S. and Goldstein J. I. 1978. Schreibersite growth and its influence on the metallography of coarse-structured iron meteorites. *Smithsonian Contributions to the Earth Sciences* 21.

Crabb J. and Anders E. 1981. Noble gases in E chondrites. *Geochimica et Cosmochimica Acta* 45:2443–2464.

Dunbar N. W., Jacobs J. K., and Naney M. T. 1995. Crystallization processes in an artificial magma: Variations in crystal shape, growth-rate, and composition with melt cooling history. *Contributions to Mineralogy and Petrology* 120:412–425.

Dowty E. 1980. Crystal growth and nucleation theory and the numerical simulation of igneous crystallization. In *Physics of magmatic processes,* edited by Hargraves R. B. Princeton: Princeton University Press. pp. 419–485.

Ehlers K. and El Goresy A. 1988. Normal and reverse zoning in niningerite: A novel key parameter to the thermal histories of EH chondrites. *Geochimica et Cosmochimica Acta* 52:877–887.

El Goresy A. and Kullerud G. 1967. Phase relations in the system Cr-Fe-S. In *Meteorite research,* edited by Millman P. M. Dordrecht: D. Reidel. pp. 638–656.

El Goresy A. and Ehlers K. 1989. Sphalerites in EH chondrites: I. Textural relations, compositions, diffusion profiles, and pressure-temperature histories. *Geochimica et Cosmochimica Acta* 53:1657–1668.

Eugster O. 1988. Cosmic ray production rates for ^{3}He, ^{21}Ne, ^{38}Ar, ^{83}Kr, and ^{126}Xe in chondrites based on ^{81}Kr-Kr exposure ages. *Geochimica et Cosmochimica Acta* 52:1649–1662.

Floss C., Fogel R. A., Yangting L., and Kimura M. 2003. Diopside-bearing EL6 EET 90102: Insights from rare earth element distributions. *Geochimica et Cosmochimica Acta* 67:543–555.

Fogel R. A. 1995. Diopside in equilibrated enstatite chondrites: EET 90102—The first diopside-bearing EL6 chondrite (abstract). 26th Lunar and Planetary Science Conference. pp. 411–412.

Fogel R. A. 1997. On the significance of diopside and oldhamite in enstatite chondrites and aubrites. *Meteoritics & Planetary Science* 32:577–591.

Gibson E. K., Jr. and Bogard D. D. 1978. Chemical alterations of the Holbrook chondrite resulting from terrestrial weathering. *Meteoritics* 13:277–289.

Grady M. M., Wright I. P., Carr L. P., and Pillinger C. T. 1986. Compositional differences in enstatite chondrites based on carbon and nitrogen stable isotope measurements. *Geochimica et Cosmochimica Acta* 50:2700–2813.

Grossman J. N. 1998. The Meteoritical Bulletin, No. 82. *Meteoritics & Planetary Science* 33:A221–A239.

Hertogen J., Janssens M. J., Takahashi H., Morgan J. W., and Anders E. 1983. Enstatite chondrites: Trace element clues to their origin. *Geochimica et Cosmochimica Acta* 47:2241–2255.

Heymann D. 1967. On the origin of hypersthene chondrites: Ages and shock effects of black chondrites. *Icarus* 6:189–221.

Heymann D. and Anders E. 1967. Meteorites with short cosmic ray exposure ages, as determined from their Al^{26} content. *Geochimica et Cosmochimica Acta* 31:1793–1809.

Hintenberger, H., Schultz L., and Wänke H. 1966. Messung der Diffusionsverluste von radiogenen und spallogenen Edelgasen in Steinmetetoriten II. *Zeitschrift für Naturforschung* 19A:1147–1159.

Kallemeyn G. W. and Wasson J. T. 1986. Compositions of enstatite (EH3, EH4, 5, and EL6) chondrites: Implications regarding their formation. *Geochimica et Cosmochimica Acta* 50:2153–2164.

Keil K. 1968. Mineralogical and chemical relationships among enstatite chondrites. *Journal of Geophysical Research* 73:6945–6976.

Keil K. 1989. Enstatite meteorites and their parent bodies. *Meteoritics* 24:195–208.

Kong P. and Ebihara M. 1996. Metal phases of L chondrites: Their formation and evolution in the nebula and in the parent body. *Geochimica et Cosmochimica Acta* 60:2667–2680.

Kong P., Mori T., and Ebihara M. 1997. Compositional continuity of enstatite chondrites and implications for heterogeneous accretion of the enstatite chondrite parent body. *Geochimica et Cosmochimica Acta* 61:4895–4914.

Kring D. A., Swindle T. D., Britt D. T., and Grier J. A. 1996. Cat Mountain: A meteoritic sample of an impact-melted asteroid regolith. *Journal of Geophysical Research* 101:29353–29371.

Kruse H. 1979. Spectra processing with computer graphics (abstract). Conference on Computers in Activation Analalyses and Gamma-Ray Spectroscopy. pp. 2228.

Larimer J. W. and Bartholomay M. 1979. The role of carbon and oxygen in cosmic gases: Some applications to the chemistry of mineralogy of enstatite chondrites. *Geochimica et Cosmochimica Acta* 43:1455–1466.

Lavrentjeva Z. A. and Lyul A. Y. 2003. REE and some other trace element distributions of mineral constituents in enstatite meteorites (abstract #1026). 34th Lunar and Planetary Science Conference. CD-ROM.

Lin Y. and El Goresy A. 2002. A comparative study of opaque phases in Qingzhen (EH3) and MacAlpine Hills 88136 (EL3): Representatives of EH and EL parent bodies. *Meteoritics & Planetary Science* 37:577–599.

Lin Y. and Kimura M. 1997. Thermal histories and parent body(ies) of EH chondrites: Evidence from new highly equilibrated EHs (Y-793225, 82189, 8404, 8414, and 86004) (abstract). 28th Lunar and Planetary Science Conference. pp. 817–818.

Lin Y. and Kimura M. 1998. Petrographic and mineralogical study of new EH melt rocks and a new enstatite chondrite grouplet. *Meteoritics & Planetary Science* 33:501–511.

Loeken T., Scherer P., Weber H. W., and Schultz L. 1992. Noble gases in eighteen stone meteorites. *Chemie der Erde* 52:249–259.

McCoy T. J., Keil K., Bogard D. D., Garrison D. H., Casanova I., Lindstrom M. M., Brearley A. J., Kehm K., Nichols R. H., Jr., and

Hohenberg C. M. 1995. Origin and history of impact-melt rocks of enstatite chondrite parentage. *Geochimica et Cosmochimica Acta* 59:161–175.

Nagel H. J., Lin Y. T., and El Goresy A. 1989. Sphalerite compositions in meteorites: A dilemma of an originally promising cosmobarometer (abstract). *Meteoritics* 24:A307.

Nickel E. H. 1992. Solid solutions in mineral nomenclature. *Canadian Mineralogist* 30:231–234.

Onorato P. I. K., Uhlmann D. R., and Simonds C. H. 1978. The thermal history of the Manicouagan impact melt sheet, Quebec. *Journal of Geophysical Research* 83:2789–2798.

Ostertag R. and Stöffler D. 1982. Thermal annealing of experimentally shocked feldspar crystals. Proceedings, 13th Lunar and Planetary Science Conference. pp. A457–A463.

Ott U. 2002. Noble gases in meteorites—Trapped components. In *Noble gases in geochemistry and cosmochemistry,* edited by Porcelli D., Ballentine C. J., and Wieler R. Washington D.C.: Mineralogical Society of America. pp. 71–96.

Ozima M., Wieler R., Marty B., and Podosek F. A. 1998. Comparative studies of solar, Q-gases, and terrestrial noble gases, and implications on the evolution of the solar nebula. *Geochimica et Cosmochimica Acta* 62:301–314.

Patzer A. and Schultz L. 2001. Noble gases in enstatite chondrites I: Exposure ages, pairing, and weathering effects. *Meteoritics & Planetary Science* 36:947–961.

Patzer A. and Schultz L. 2002. Noble gases in enstatite chondrites II: The trapped component. *Meteoritics & Planetary Science* 37: 601–612.

Patzer A., Hill D. H., and Boynton W. V. 2004. Evolution and classification of acapulcoites and lodranites from a chemical point of view. *Meteoritics & Planetary Science* 39:61–85.

Pouchon J. L. and Pichoir F. 1991. Quantitative analysis of homogenous or stratified microvolumes applying the model "PAP." In *Electron probe quantitation,* edited by Heinrich K. F. J. and Newbury D. E. New York: Plenum Press. pp. 31–75.

Ramdohr P. 1963. The opaque minerals in stony meteorites. *Journal of Geophysical Research* 68:2011–2036.

Ramdohr P. 1973. *The opaque minerals in stony meteorites.* Amsterdam/London/New York: Elsevier Publishing Company. 245 p.

Romig A. D. and Goldstein J. I, Jr. 1981. Low temperature phase equilibria in the Fe-Ni and Fe-Ni-P systems: Application to the thermal history of metallic phases in meteorites. *Geochimica et Cosmochimica Acta* 45:1187–1197.

Rubin A. E. 1994. Metallic copper in ordinary chondrites. *Meteoritics* 29:93–98.

Rubin A. E. 1997a. The Galim LL/EH polymict breccia: Evidence for impact-induced exchange between reduced and oxidized meteorite matter. *Meteoritics & Planetary Science* 32:489–492.

Rubin A. E. 1997b. Sinoite (Si_2N_2O): Crystallization from EL chondrite impact melts. *American Mineralogist* 82:1001–1006.

Rubin A. E. 1997c. Igneous graphite in chondritic meteorites. *Mineralogical Magazine* 61:699–703.

Rubin A. E. and Scott E. R. D. 1997. Abee and related EH chondrite impact-melt breccias. *Geochimica et Cosmochimica Acta* 61: 425–435.

Rubin A. E., Scott E. R. D., and Keil K. 1997. Shock metamorphism of enstatite chondrites. *Geochimica et Cosmochimica Acta* 61: 847–858.

Scherer P., Schultz L., and Loeken T. 1994. Weathering and atmospheric noble gases in chondrites. In *Noble gas geochemistry and cosmochemistry,* edited by Matsuda J. Tokyo: Terra Scientific Publishing Company. pp. 43–53.

Scherer P., Herrmann S., and Schultz L. 1998. Noble gases in twenty-one Saharan LL chondrites: Exposure ages and possible pairings. *Meteoritics & Planetary Science* 33:259–265.

Schmitt R. T. 2000. Shock experiments with the H6 chondrite Kernouvé: Pressure calibration of microscopic shock effects. *Meteoritics & Planetary Science* 35:545–560.

Schultz L. and Weber H. 1995. Exposure ages of H chondrites with helium loss (abstract). *Meteoritics* 30:575–576.

Schultz L. and Weber H. 1997. Exposure age distribution of H chondrites with and without helium loss (abstract). In *Isotopes in the solar system.* Ahmedabad: Physical Research Laboratory. pp. 34–35.

Schultz L., Scherer P., Spettel B., Wlotzka F., Zipfel J., Schlüter J., Merchel S., Herpers U., Newton J., Franchi I. A., Pillinger C. T., Leya I., Neumann S., Neupert U., Michel R., Kubik P. W., Synal H. A., Bonani G., Hajdas I., Ivy-Ochs S., and Suter M. 1998. Ten new meteorites from the Ténéré desert (Niger): Classification, noble gases, cosmogenic nuclides, and terrestrial ages (abstract). *Meteoritics & Planetary Science* 33:A138.

Sears D. W. G. 1980. Formation of E chondrites and aubrites—A thermodynamic model. *Icarus* 43:184–202.

Sears D. W. G., Kallemeyn G. W., and Wasson J. T. 1982. The compositional classification of chondrites—II. The enstatite chondrite groups. *Geochimica et Cosmochimica Acta* 46:597–608.

Spry A. 1969. *Metamorphic textures.* Oxford: Pergamon Press. 350 p.

Stöffler D., Keil K., and Scott E. R. D. 1991. Shock metamorphism of ordinary chondrites. *Geochimica et Cosmochimica Acta* 55: 3845–3867.

Swindle T. D. 1988. Trapped noble gases in meteorites. In *Meteorites and the early solar system,* edited by Kerridge J. F. and Matthews M. S. Tucson: University of Arizona Press. pp. 535–564.

Tarkian M. and Bernhardt H. J. 1984. A key diagram for the optical determination of platinum-group minerals. *Tschermaks Mineralogische und Petrologische Mitteilungen* 33:121–129.

Van Schmus W. R. and Wood J. A. 1967. A chemical-mineralogical classification for the chondrite meteorites. *Geochimica et Cosmochimica Acta* 31:747–765.

Vogt S., Herzog G. F., and Reedy R. C. 1990. Cosmogenic nuclides in extraterrestrial materials. *Reviews in Geophysics* 28:253–275.

Wasson J. T. and Kallemeyn G. W. 1988. Composition of chondrites. *Reviews in Geophysics* 10:711–759.

Weeks K. S. and Sears D. W. G. 1985. Chemical and physical studies of type 3 chondrites—V: The enstatite chondrites. *Geochimica et Cosmochimica Acta* 49:1525–1536.

Wieler R. 2002. Cosmic ray-produced noble gases in meteorites. In *Noble gases in geochemistry and cosmochemistry,* edited by Porcelli D., Ballentine C. J., and Wieler R. Washington D.C.: Mineralogical Society of America. pp. 125–170.

Zhang Y., Benoit P. H., and Sears D. W. G. 1995. The classification and complex thermal history of the enstatite chondrites. *Journal of Geophysical Research* 100:9417–9438.

Zipfel J., Scherer P., Spettel B., Dreibus G., and Schultz L. 2000. Petrology and chemistry of the new shergottite Dar al Gani 476. *Meteoritics & Planetary Science* 35:95–106.